
Master's thesis
Theoretical physics

# The search for the charged Higgs boson and a tau veto in the event selection

Joona Havukainen
2016

| | |
|---|---|
| Advisor: | Dr. Sami Lehti |
| Examiners: | Dr. Sami Lehti |
| | Prof. Paula Eerola |

HELSINGIN YLIOPISTO
FYSIIKAN LAITOS

PL 64 (Gustaf Hällströmin katu 2)
00014 Helsingin yliopisto

HELSINGIN YLIOPISTO — HELSINGFORS UNIVERSITET — UNIVERSITY OF HELSINKI

| Tiedekunta/Osasto — Fakultet/Sektion — Faculty | Laitos — Institution — Department |
|---|---|
| Faculty of Science | Department of Physics |

Tekijä — Författare — Author
Joona Havukainen

Työn nimi — Arbetets titel — Title

The search for the charged Higgs boson and a tau veto in the event selection

| Oppiaine — Läroämne — Subject | | |
|---|---|---|
| Theoretical physics | | |
| Työn laji — Arbetets art — Level | Aika — Datum — Month and year | Sivumäärä — Sidoantal — Number of pages |
| Master's thesis | May 2016 | 75 |

Tiivistelmä — Referat — Abstract

After the finding of a Higgs boson at the Large Hadron Collider of CERN, the next milestone in experimental particle physics is the detection of a new particle beyond the Standard Model. Many of the popular extensions of the Standard Model are so called Two-Higgs-doublet models, that include five physical Higgs bosons in total. Two of the bosons are neutral scalars, two are charged scalars and one is a pseudoscalar.

The first part of this thesis presents the Standard Model of particle physics as a gauge field theory where the gauge principle is used to introduce interactions between the particles. Quantum electrodynamics, weak interactions and quantum chromodynamics with their properties are discussed. The electroweak symmetry breaking through the Higgs mechanism and its implications for the masses of the particles are shown. The considerations on the Standard Model are concluded by discussing some of the problems in the Standard Model.

Supersymmetric extensions to the Standard Model are introduced, motivated by their potential to solve some of the problems and by the framework for new physics the supersymmetry provides. The Higgs sector in the more constrained minimal supersymmetry scenario is discussed and some of the properties for these new Higgs bosons are given.

The latter part of the thesis focuses on the experimental aspects of high energy particle physics. The search for the charged Higgs boson in the $H^+ \to \tau^+ \nu_\tau$ decay channel, with the tau lepton decaying into hadronic decay products is presented in detail. Vetoing collision events with more than one tau particle is shown to enhance the transverse mass resolution of the analysis, improving the signal detection. Methods for performing a tau veto are discussed and the problems in performing the tau veto are studied using 13 TeV collision event simulations and data from 2015 from the CMS detector at the LHC. No viable way of performing the tau veto in such a way that it improves the overall analysis is found.

Avainsanat — Nyckelord — Keywords
charged Higgs boson

Säilytyspaikka — Förvaringsställe — Where deposited
Kumpula campus library

Muita tietoja — övriga uppgifter — Additional information

# Contents


**1 Introduction** **3**

**2 The Standard Model of particle physics** **5**
2.1 Particle content and gauge symmetries . . . . . 5
2.2 Quantum Electrodynamics . . . . . 7
2.3 The weak interaction and the electroweak unification . . . . . 12
2.4 Spontaneous Symmetry Breaking and the Higgs boson . . . . . 17
2.5 Quantum Chromodynamics . . . . . 23
2.6 Problems of the Standard Model . . . . . 27

**3 Supersymmetry** **29**
3.1 A new symmetry of space-time . . . . . 29
3.2 Two Higgs-doublet models . . . . . 32
3.2.1 The Higgs sector in minimal supersymmetric models . . . . . 32

**4 Studying physics with collider experiments** **34**
4.1 The coordinate system . . . . . 34
4.2 Useful quantities in collider experiments . . . . . 35
4.3 Structure of the proton . . . . . 36

**5 The Large Hadron Collider and the CMS detector** **39**
5.1 Structure of the accelerator . . . . . 39
5.2 The CMS detector . . . . . 40

**6 Reconstructing collision data** **45**
6.1 Particle-Flow event reconstruction . . . . . 45
6.2 $\tau$-jet reconstruction . . . . . 48

**7 Searching for the Charged Higgs boson in the $H^{\pm} \to \tau^{\pm}\nu$ fully hadronic -channel** **50**
7.1 Signal . . . . . 50
7.2 Backgrounds . . . . . 52
7.3 Event selection . . . . . 53
7.4 Tau veto . . . . . 54

**8 Results** **56**
8.1 Statistical significance and systematic uncertainties . . . . . 56
8.1.1 An optimistic tau veto using charged tracks . . . . . 58
8.1.2 A realistic veto using isolated charged tracks and tau identification . . . . . 64

**9 Conclusions** **66**

**Bibliography** **66**

**Appendix** **74**

# Chapter 1

# Introduction

After the finding of a Higgs boson in the Large Hadron Collider at CERN in 2012 [1], [2], the focus has shifted into searching physics beyond the Standard Model of particle physics. Even though phenomenally successful, the Standard Model is certainly not the complete model of particle physics, as there are observations that are not commented upon by the Standard Model framework at all. Many theories extend the Standard Model in order to include new physics such as possible candidates for dark matter or to solve existing troublesome aspects of the model like the hierarchy problem. Since observations act as the final judge on which theory is correct, the hunt for new experimental evidence of the physics beyond the Standard Model intensifies. The finding of another scalar boson such as the charged Higgs boson would give a strong sense of direction in the search for the improved theory of particle physics.

In the first part of this thesis I present the Standard Model as a gauge field theory with the emphasis on the powerful concept of symmetries and how they introduce interactions between the free gauge fields. With this approach the electric, weak and strong interactions are constructed in a generalized way and their properties are shown to come from the underlying symmetry group of the Lagrangian describing the particles. The bare masses of the particles are shown to come through a mechanism of Spontaneous Symmetry Breaking, allowing the theory to have massive particles and remain renormalizable as physical theories are expected to. After constructing the Standard Model, I will comment on its shortcomings as a motivation for the extensions to the Standard Model.

The concept of supersymmetry is presented, offering fixes for many theoretical problems of the Standard Model and providing rich foundation for including new physics into the model. The Higgs sector of supersymmetric models is bound to include at least five Higgs bosons in order to match the observed physics of the Standard Model. The reasons for extending the Higgs sector and some considerations for the properties of the new Higgs bosons will be presented as a conclusion to the theory part of the thesis.

In the second part of the thesis I talk about the experimental search for these theoretical new Higgs bosons of at the Compact Muon Solenoid detector at the Large Hadron Collider of CERN. This includes description of the Large Hadron Collider and the Compact Muon Solenoid detector, general overview of hadron acceleration and collisions and the reconstruction of the physical events in the hadron collisions from the data of the detector. An overview of the simulating these particle collisions using Monte Carlo methods is also given. After these considerations, one search channel for the charged Higgs bosons is discussed in more detail and my own work using simulations to study the viability of

an algorithm to reduce some of the background events at the center of mass energy of 13 TeV is presented.

# Chapter 2

# The Standard Model of particle physics

The description of all the known particles and their interactions constituting the visible matter of the universe, is given by the so called Standard Model of particle physics (SM). It accommodates the theories and observations of quantum mechanics and special relativity, describing particles as excitations of quantum fields. The construction of the SM was a long pursuit that continued throughout the 20th century, inspired by the *Noether's theorems* [3] that relate every continuous symmetry of a physical system to correspond to a conserved quantity. By symmetry it is meant that a system can be altered in some way while keeping the equations of motion invariant. In this chapter I present the main components of the SM and how they are generated by symmetries. I also discuss the symmetry breaking in the electroweak sector, resulting in bare masses for the particles through the Higgs mechanism. At the end of the chapter, the known problems of the SM are presented as a motivation for the discussion of the Beyond the Standard Model (BSM) theories in Chapter 3.

The methods for calculating the observables such as scattering amplitudes and lifetimes of particles for quantum fields are presented in [4]. The emphasis is put in generating the dynamical theory of interacting quantum fields by the use of symmetries. The Lagrangians give the equations of motions for the interacting particles and ultimately the framework for calculating the desired observables from the theory is constructed from them. This approach shows how the different types of symmetries of the Lagrangian give the different interactions their properties.

The concept of *renormalization* is the process of systematically treating infinities that might arise in the calculations of a theory. The theories describing nature are expected to be renormalizable since bare infinities in any measurable quantities are not observed in Nature and it should not bode well if a theory gives a prediction of such an observable. The Standard Model is renormalizable to any order of perturbation, owing much to the method of including masses to the particles through Spontaneous Symmetry Breaking (SSB) that will be described later and a proof that before the inclusion of masses, the massless gauge fields are renormalizable, as was shown by Gerard t'Hooft [5].

## 2.1 Particle content and gauge symmetries

The existing matter particles known as *fermions* cannot be derived from the first principles of the theory, but need to be taken from observations in most cases. One exception from

this could be said to be the prediction of the third generation of quarks, containing the t- and b-quarks. The study of CP-violation [6] in renormalizable theory for weak interaction lead M. Kobayashi and T. Maskawa to suggest a new generation of particles in 1972, and the prediction was confirmed experimentally over the following decades with evidence for $\tau$ lepton in 1975 [7] and the discovery in 1977 [8] at SLAC, the observation of b-quark in 1977 at Fermilab [9] and the observation of t-quark in 1995 at Fermilab [10]. However the four other quarks and the two leptons were already found by then and this prediction would not have been possible without prior knowledge of existing generations of particles. The known fermions are taken as the given particle content of the theory and used as the building blocks for the Standard Model. The interaction mediating particles called *bosons* will be shown to come into the theory through the symmetries of the fermion Lagrangians describing their equations of motion. The fermions and bosons are represented in Figure (2.1), fermions on the three leftmost columns, bosons in the rest. There exists also antiparticles for each of the fermions, that are not shown in this figure. More on each type of particles is said in the following sections on interactions between the particles.

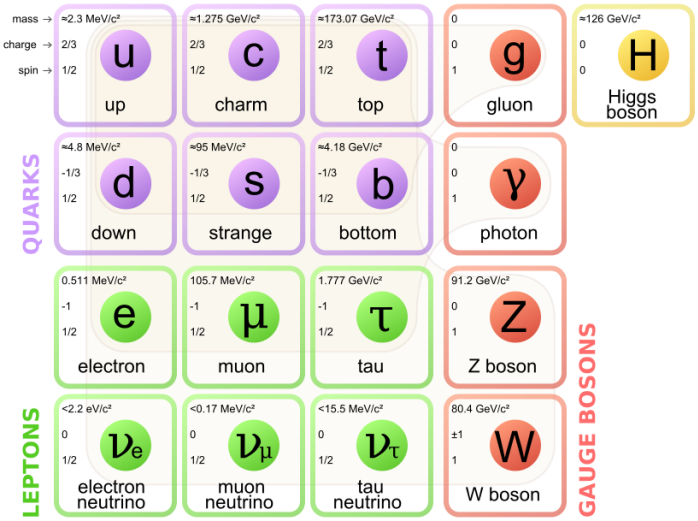


Figure 2.1: The particles of the Standard Model. Three generations of fermions in the columns on the left and the bosons in the remaining two [11].

In quantum field theories, the fields themselves are not the observable quantities, but rather their excitations such as the particles and their properties in the SM. So two fields that produce the same observables are indiscernible to our experiments. We must therefore take into account the fact that the fields have some freedom that we cannot constrain with observations. If we have two different fields that generate the same physics, we call the transformation from one of these fields to the other a *gauge transformation* and the fields are called *gauge fields*.

With this in mind, the strategy in creating a quantum field theory describing the SM is the following: First one finds the Lagrangian giving the equation of motion of the free particles

without interactions. Next by studying the free Lagrangian, a global gauge symmetry can be found. Promoting the global gauge symmetry into a local gauge symmetry and demanding the physics to remain unchanged i.e. the Lagrangian to stay invariant will give the unobservable fields the maximal amount of freedom. As I will show, this requirement for local gauge invariance will require the addition new terms on top of the original free Lagrangian terms into the theory, in order to compensate for terms arising from local gauge transformations. It turns out the correct interpretation of these new terms will be as the interactions between the fields of the theory and a new gauge field. These gauge fields give rise to new particles, the bosons that mediate forces between other particles of the original fields.

## 2.2 Quantum Electrodynamics

The description of how light and matter interact is in the realm of Quantum Electrodynamics (QED). It describes the electric charges interacting through exchanging particles of the electromagnetic field i.e. photons. The foundations of QED is often credited to Dirac and his paper with a quantum description of atoms interacting with a radiation field [12], giving results for the absorption and emission probabilities for photons. Other important steps in the development of the theory that should be mentioned were the formulation of covariant QED by Tomonaga [13], where the Lorentz invariance of the theory was demonstrated and Nobel award winning papers by Feynman [14], Schwinger [15] and Tati & Tomonaga [16] solving divergence problems in the theory, resulting in a renormalizable theory of quantum electrodynamics.

The particles of QED are the leptons and the photons. The quarks also carry an electric charge, but they are neglected for now. This means that the free fields for electrons, muons, taus and photons are included into the Lagrangian. Fortunately the leptons have the same charge and coupling to the electromagnetic field so only difference between the Lagrangians will be the mass parameters.

The correct quantum mechanical description for leptons that are charged particles with spin-$\frac{1}{2}$ is given by the Dirac equation. It was presented by Dirac in 1928 [17] and it was the first time an electron was described in the context of relativistic quantum mechanics:

$$(i\gamma^\mu \partial_\mu - m)\psi = 0, \tag{2.1}$$

where the $\gamma^\mu$ are the Dirac matrices, $m$ is the mass of the particle and $\psi$ is the Dirac four-spinor depending on $x$ i.e. $\psi = \psi(x)$, containing the wave functions for both the particle and its antiparticle i.e. electron and positron. This equation is obtained from the Lagrangian:

$$\mathcal{L}_{Dir} = i\bar{\psi}\gamma^\mu\partial_\mu\psi - m\bar{\psi}\psi = \bar{\psi}(i\partial\!\!\!/ - m)\psi, \tag{2.2}$$

with $\bar{\psi} = \gamma^0\psi$ and $\partial\!\!\!/ = \gamma^\mu\partial_\mu$. The Lagrangian gives the equation of motion, the Dirac equation, when the action is minimized by applying the Euler-Lagrange equations, a standard procedure in variational calculus:

$$\begin{aligned} &\frac{\partial\mathcal{L}}{\partial\bar{\psi}} - \frac{\partial}{\partial x^\mu}\frac{\partial\mathcal{L}}{\partial(\partial_\mu\bar{\psi})} = 0 \\ &\Leftrightarrow (i\gamma^\mu\partial_\mu - m)\psi = 0. \end{aligned} \tag{2.3}$$

The Dirac Lagrangian (2.2) is invariant under the symmetry group U(1). It consists of 1x1 unitary matrices, that is matrices satisfying $\mathbf{U}^*\mathbf{U} = \mathbf{U}\mathbf{U}^* = 1$. This is the set of all unit complex numbers $\mathrm{U}(1) = \{e^{i\theta}|\theta \in \mathbb{R}\}$, which is also called the circle group. The group is isomorphic (mathematically saying "structurally the same") to the group of orthogonal 2x2 matrices, that have the determinant of $\pm 1$, called the SO(2) or "special orthogonal group". Writing open the members of the group SO(2) as

$$\mathrm{SO}(2) = \left\{ \begin{pmatrix} \cos\theta & -\sin\theta \\ \sin\theta & \cos\theta \end{pmatrix} \middle| \theta \in \mathbb{R} \right\} \tag{2.4}$$

which shows that a symmetry operation $\mathrm{U}(1) \cong \mathrm{SO}(2)$ is then equivalent of a rotation in the complex plane $(x, i)$, giving the simple visualisation of the circle group operation as rotating a circle an angle of $\theta$ in the complex plane. Other notable attributes of the symmetry group U(1) is that its members commute with each other. Groups with this property are called *abelian groups*. For two members of an abelian group the the following relation holds:

$$\mathrm{U}(\theta_1)\mathrm{U}(\theta_2) = e^{i\theta_1}e^{i\theta_2} = e^{i\theta_2}e^{i\theta_1} = \mathrm{U}(\theta_2)\mathrm{U}(\theta_1). \tag{2.5}$$

Now imposing the U(1) symmetry upon the Lagrangian for the leptons in order to show the gauge invariance explicitly. This is done by making the gauge transformation

$$\begin{aligned} \psi &\to \psi' = e^{-ie\alpha}\psi \\ \bar{\psi} &\to \bar{\psi}' = e^{ie\alpha}\psi \end{aligned}$$

where $e$ in the exponential is just a constant. The letter $e$ is chosen as it will be the elementary electric charge in the theory. The Lagrangian remains invariant under this global transformation as

$$\begin{aligned}\mathcal{L}_{Dir} \rightarrow \mathcal{L'}_{Dir} =& e^{ie\alpha}\bar{\psi}(i\not{\partial} - m)e^{-ie\alpha}\psi \\ =& e^{ie\alpha}e^{-ie\alpha}\bar{\psi}(i\not{\partial} - m)\psi \\ =& \bar{\psi}(i\not{\partial} - m)\psi \\ \Leftrightarrow \mathcal{L}_{Dir} =& \mathcal{L'}_{Dir}\end{aligned}$$

This global symmetry is promoted to a local one by allowing $\alpha$ to depend on $x$. The new transformations are

$$\begin{aligned}\psi \rightarrow \psi' &= e^{-ie\alpha(x)}\psi \\ \bar{\psi} \rightarrow \bar{\psi}' &= e^{ie\alpha(x)}\psi\end{aligned}$$

and with these transformations the Lagrangian becomes

$$\begin{aligned}\mathcal{L'}_{Dir} =& e^{ie\alpha(x)}\bar{\psi}(i\not{\partial} - m)e^{-ie\alpha(x)}\psi \\ =& e^{ie\alpha(x)}e^{-ie\alpha(x)}\bar{\psi}(i\not{\partial} - m)\psi - \bar{\psi}(i^2 e\gamma^\mu\psi\partial_\mu\alpha(x)) \\ =& \mathcal{L}_{Dir} + e\bar{\psi}\gamma^\mu\psi\partial_\mu\alpha(x).\end{aligned}$$

So with the promotion of a global gauge invariance into a local one, the Lagrangian picked up an extra term due to the partial derivative. The odd looking term can be removed by introducing a new gauge field $A^\mu$ into the equations through the redefinition of the partial derivative as the *covariant derivative*:

$$\partial_\mu \rightarrow D_\mu = \partial_\mu + ieA_\mu. \tag{2.6}$$

The excess term is removed by demanding the new gauge field $A^\mu$ to transform as

$$A_\mu \rightarrow A'_\mu = A_\mu + \partial_\mu\alpha(x) \tag{2.7}$$

under the U(1) transformations. Now when performing the local transformation on the Lagrangian where the partial derivative is replaced by the covariant derivative, one gets

$$\begin{aligned}\mathcal{L'}_{Dir} =& \mathcal{L}_{Dir} + e\bar{\psi}\gamma^\mu\psi\partial_\mu\alpha(x) - e\bar{\psi}\gamma^\mu\psi\partial_\mu\alpha(x) - e\bar{\psi}\gamma^\mu\psi A_\mu \\ =& \mathcal{L}_{Dir} + \mathcal{L}_{int},\end{aligned}$$

where $\mathcal{L}_{int} = -e\bar{\psi}\gamma^\mu\psi A_\mu$. Unlike the term with $\partial_\mu\alpha(x)$ that was gotten rid of by introducing a new gauge field, this term is understood as interaction between the fields $\psi, \bar{\psi}$ and $A^\mu$. This is due to the formulation of quantum field theory, where the fields are promoted into operators that create and annihilate particles. The new term $\mathcal{L}_{int}$ is interpreted as a particle of field $A^\mu$ interacting with a particle from field $\bar{\psi}$ and a particle from $\psi$. It can be represented diagrammatically as a *Feynman diagram*, shown in Figure (2.2).

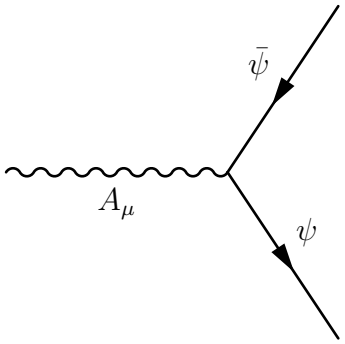


Figure 2.2: A Feynman graph describing the interaction term $\mathcal{L}_{int} = -e\bar{\psi}\gamma^\mu\psi A_\mu$. The constant $e$ characterizes the strength of the interaction, being the elementary charge.

The nature of the gauge field $A_\mu$ has to be inspected. The only knowledge available of it is how it transforms under $U(1)$ and that it is a vector field. However, as the QED is designed to describe interactions of light and matter, a candidate of interest is the electromagnetic four-potential $A^\mu = (\frac{\phi}{c}, \vec{A})$ where $\phi$ is the electric potential and $\vec{A}$ is the magnetic vector potential. Writing the electric and magnetic fields in terms of this four potential

$$\begin{aligned}\vec{E} =& -\nabla\phi - \frac{\partial\vec{A}}{\partial t}\\ \vec{B} =& \nabla\times\vec{A}.\end{aligned}$$

An antisymmetric tensor $F^{\mu\nu}$ can be defined as

$$F^{\mu\nu} \equiv \partial^\mu A^\nu - \partial^\nu A^\mu = \begin{bmatrix} 0 & -E_x & E_y & E_z \\ E_x & 0 & -B_z & B_y \\ E_y & B_z & 0 & -B_z \\ E_z & -B_y & B_x & 0 \end{bmatrix} \tag{2.8}$$

and the Maxwell's equations describing electromagnetism in the inhomogeneous case can be written as

$$\partial_\mu F^{\mu\nu} = J^\nu, \tag{2.9}$$

where $J^\nu = (\rho, \vec{J})$ is the four-current containing charge density $\rho$ and current density $\vec{J}$. The Maxwell's equations are the equations of motion describing the electromagnetic fields with some sources $J^\nu$. These equations are derived from the Lagrangian of the form

$$\mathcal{L}_\gamma = -\frac{1}{4} F^{\mu\nu} F_{\mu\nu}. \tag{2.10}$$

This inner product of two tensors is manifestly Lorentz invariant and it also possesses gauge invariance under the transformation

$$A^\mu \to A'^\mu = A^\mu + \partial^\mu \alpha(x), \tag{2.11}$$

as can be seen from:

$$\begin{aligned}
\mathcal{L} \to \mathcal{L}' =& -\frac{1}{4} F'^{\mu\nu} F'_{\mu\nu} \\
=& -\frac{1}{4} (\partial^\mu A'^\nu - \partial^\nu A'^\mu)(\partial_\mu A'_\nu - \partial_\nu A'_\mu) \\
=& -\frac{1}{4} (\partial^\mu [A^\nu + \partial^\nu \alpha(x)] - \partial^\nu [A^\mu + \partial^\mu \alpha(x)])(\partial_\mu [A_\nu + \partial_\nu \alpha(x)] - \partial_\nu [A_\mu + \partial_\mu \alpha(x)]) \\
=& -\frac{1}{4} (\partial^\mu A^\nu - \partial^\nu A^\mu)(\partial_\mu A_\nu - \partial_\nu A_\mu) - \frac{1}{4} (\partial^\mu \partial^\nu \alpha(x) - \partial^\nu \partial^\mu \alpha(x))(\partial_\mu \partial_\nu \alpha(x) - \partial_\nu \partial_\mu \alpha(x)) \\
=& -\frac{1}{4} (\partial^\mu A^\nu - \partial^\nu A^\mu)(\partial_\mu A_\nu - \partial_\nu A_\mu) \\
\Leftrightarrow& \mathcal{L}' = \mathcal{L}.
\end{aligned}$$

So the electromagnetic four-potential in the Lagrangian describing the photons has the same transformation qualities as the vector field $A^\mu$ that was added to the Dirac Lagrangian in order to conserve invariance under local gauge transformations. As the photons are needed to complete the Lagrangian of the QED, $A^\mu$ in the Dirac Lagrangian should be interpreted as the electromagnetic four-potential and the kinetic term $\mathcal{L}_\gamma$ added to the total QED Lagrangian in order for the photons to be able to propagate. Now the QED Lagrangian is written as:

$$\begin{aligned}
\mathcal{L}_{QED} &= \mathcal{L}_{Dir} + \mathcal{L}_\gamma + \mathcal{L}_{int} \\
&= \bar{\psi}(i\partial\!\!\!/ - m)\psi - \frac{1}{4} F^{\mu\nu} F_{\mu\nu} - e\bar{\psi}\gamma^\mu A_\mu \psi
\end{aligned} \tag{2.12}$$

The leptons have the same coupling strength and charge, so in order to add muons and taus to the QED, one can simply write a sum over the leptonic terms as

$$\mathcal{L}_{QED} = \sum_{i=1}^{3} \left( \bar{\psi}_i (i\partial\!\!\!/ - m_i)\psi_i - e\bar{\psi}_i \gamma^\mu A_\mu \psi_i \right) - \frac{1}{4} F^{\mu\nu} F_{\mu\nu}, \tag{2.13}$$

where i=1, 2, 3 represent electron, muon and tauon respectively. This gives the description of leptons interacting via exchange of photons.

The QED was the first part of the Standard Model to be discovered. The gauge bosons of the QED are not restricted but have a long interaction range and as such, photons were very well known before the theory was formulated. The relatively weak coupling strength makes perturbative calculations possible and the observables can be calculated with the perturbation theory and compared with experiments. Structurally the theory is simple at least when compared to the other interactions. This is due to the symmetry group U(1) and its abelian nature. The case for weak and strong interactions will be different as their symmetry groups are non-abelian.

## 2.3 The weak interaction and the electroweak unification

The weak interaction makes reactions like nuclear fusion and fission possible, being responsible for the interactions between the quarks required to transform the nuclei. The weak interaction couples to all the fermions in the Standard Model. The first theory trying to explain the weak interaction for the $\beta$ -decay was made by Enrico Fermi in 1933 with his four-fermion interaction model [18], and it could also be applied to the muon decay with good results. Regardless of the model's success in low energies where the interaction indeed looks like a four-particle interaction, when probing smaller distances the interaction is revealed to be different. This is because the interaction is mediated by massive vector bosons, restricting the interaction to short distances as the bosons decay quickly. Such short ranges make the interaction seem like a contact interaction of four-particles at low energies.

Another notable difference to the electromagnetic interaction is the violation of parity conservation of the interacting particles. Parity means the inversion of a coordinate in a physical system by a parity operator $\mathcal{P}$, for example in a wavefunction describing a particle $\phi(x) \xrightarrow{\mathcal{P}} \phi(-x)$. This property for the weak interaction was proposed by T.Lee and C.Yang [19] in 1956 and confirmed in the following years by experiments. This leads to an unequal setting for the *left-handed* and *right-handed* particles of the Standard Model, where by handedness one refers to an intrinsic property of the particle called the *chirality*, that every particle of non-integer spin has. Chirality is defined by the transformation properties of a particle under the Dirac gamma matrix $\gamma^5$, under which the fermions have eigenvalues $\pm 1$:

$$\gamma^5 = \begin{pmatrix} 0 & 0 & 1 & 0 \\ 0 & 0 & 0 & 1 \\ 1 & 0 & 0 & 0 \\ 0 & 1 & 0 & 0 \end{pmatrix}. \tag{2.14}$$

The positive and negative eigenvalues correspond to the right- and left-handed particles respectively. As a result of this parity violation, only left-handed particles interact with $W^{\pm}$ bosons that mediate the *charged current* weak interaction. As a consequence there are no right-handed neutrinos in the Standard Model, as they could only interact through gravity. Other right-handed particles do however interact through *neutral current* weak interactions, coupling to a $Z^0$ boson.

The weak interaction also violates the charge-parity conservation, making particles and antiparticles behave differently as was observed in decays of $K^0$ mesons by J.Christenson *et al.* in 1964 [20]. This is an important feature as any sort of asymmetry between the particles and their antiparticle partners might help explain the baryon asymmetry of the Universe, which will be commented on at the end of this chapter.

In order to accommodate these features in the theory, the fields describing the particles need to be separated by their chirality or handedness. This will also result in a theory that will be non-Abelian i.e. the gauge transformations of the symmetry group do not commute trivially. This in turn leads to interactions between the gauge particles themselves, unlike what was seen in the QED photons. Starting with definitions of the left- and right-handed fields as

$$\psi = \psi_L + \psi_R \tag{2.15}$$

where

$$\psi_L = P_L\psi = \frac{(1-\gamma_5)}{2}\psi$$
$$\psi_R = P_R\psi = \frac{(1+\gamma_5)}{2}\psi.$$

The projection operators $P_L$, $P_R$ pick out left and right chirality states of fermionic fields and satisfy the usual requirements for projection operators:

$$P_R P_R = P_R, \quad P_L P_L = P_L, \quad P_L P_R = P_R P_L = 0. \tag{2.16}$$

This allows the separation the Lagrangian into left- and right-handed components

$$\begin{aligned}\mathcal{L}_{leptons} &= \mathcal{L}_L + \mathcal{L}_R \\ &= \sum_{i=1}^{3} \left( \bar{\psi}_i^L (i\partial\!\!\!/ - m)\psi_i^L + \bar{\psi}_i^R (i\partial\!\!\!/ - m)\psi_i^R \right),\end{aligned} \tag{2.17}$$

where i=1,2,3 correspond to electrons, muons and tauons respectively. The $\psi_i^L$ contain the left-handed fields as doublets and $\psi_i^R$ the right-handed fields as singlets:

$$\psi_1^L = \begin{pmatrix} \nu_e \\ e \end{pmatrix}, \;\; \psi_2^L = \begin{pmatrix} \nu_\mu \\ \mu \end{pmatrix}, \;\; \psi_3^L = \begin{pmatrix} \nu_\tau \\ \tau \end{pmatrix}, \quad \psi_1^R = e, \;\; \psi_2^R = \mu, \;\; \psi_3^R = \tau, \tag{2.18}$$

where the right-handed neutrinos are discarded. This gives the basis for building a structure where there are interactions between the left-handed leptons and their neutrinos but no interactions between right-handed leptons and neutrinos, as the parity violation requires.

The Lagrangian (2.16) is invariant under transformations of the form

$$\psi_i \to \mathbf{U}\psi_i, \quad \bar{\psi}_i \to \bar{\psi}_i \mathbf{U}^\dagger, \tag{2.19}$$

where the $\mathbf{U}$ are 2x2 matrices fulfilling the conditions

$$\mathbf{U}\mathbf{U}^\dagger = \mathbf{U}^\dagger\mathbf{U} = \mathbb{1}, \quad \det(\mathbf{U}) = 1. \tag{2.20}$$

The matrices for the transformations fulfilling the above conditions belong to the Lie group SU(2). The group has three dimensions, meaning that we need three linearly independent generators for this group of transformations. The Lagrangian is invariant with respect to any of these, predicting three separate gauge fields to appear as these global invariances are promoted into local invariances. The Lagrangian of this form is also invariant under transformations of the Lie group U(1) as was shown in the case of QED, resulting in one more gauge boson. Here I am assuming that the leptons interact identically, after corrected for the mass differences between fermions. This concept is known as the *lepton universality* and it has so far been shown to hold within experimental accuracy, for example by experiments at LEP of CERN [21].

An SU(n) matrix can be written as an exponential

$$\mathbf{U} = e^{i\omega_a T^a}, \tag{2.21}$$

where $\omega_a$ are real parameters and $T^a$ are the generators of the Lie group. The number of generators is equal to the dimension of the group, so for SU(2) there will be three generators. Allowing U to depend on $x$:

$$\begin{aligned}\mathcal{L} \to \mathcal{L}' &= \bar{\psi}_i U^\dagger(x)(i\partial\!\!\!/ - m_i)U(x)\psi_i \\ &= \bar{\psi}_i(i\partial\!\!\!/ - m_i)\psi_i + i\bar{\psi}_i U^\dagger(x)(\partial\!\!\!/ U(x))\psi_i.\end{aligned} \tag{2.22}$$

The extra term is removed by defining the covariant derivate as

$$D_\mu = \partial_\mu \mathbb{1} + igW_\mu, \tag{2.23}$$

where $W_\mu$ can be written in component form with the generators as the basis $W_\mu = W_\mu^a T_a$ and $g$ is a coupling constant. The new gauge field $W_\mu$ now has to transform as

$$W_\mu \to U(x)W_\mu U^\dagger(x) + \frac{i}{g}(\partial_\mu U(x))U^\dagger(x), \tag{2.24}$$

to cancel the excess term. Writing the Lagrangian with this covariant derivative, it is shown that

$$\begin{aligned}\mathcal{L} &= \bar{\psi}_i(iD\!\!\!/ - m_i)\psi_i \\ \to \mathcal{L}' &= \bar{\psi}_i(i\partial\!\!\!/ - m_i)\psi_i + i\bar{\psi}_i U^\dagger(\partial\!\!\!/ U)\psi_i - i\bar{\psi}_i U^\dagger U U^\dagger(\partial\!\!\!/ U)U^\dagger U\psi_i \\ &\quad - g\bar{\psi}U^\dagger U\gamma^\mu W_\mu^i U^\dagger U\psi \\ &= \bar{\psi}_i(i\gamma^\mu(\partial + igW_\mu^i) - m_i)\psi_i + i\bar{\psi}_i U^\dagger(\partial\!\!\!/ U)\psi_i - i\bar{\psi}_i U^\dagger(\partial\!\!\!/ U)\psi_i \\ &= \bar{\psi}_i(iD\!\!\!/ - m_i)\psi_i \\ \leftrightarrow \mathcal{L} &= \mathcal{L}'.\end{aligned} \tag{2.25}$$

In order to write the covariant derivative explicitly, the generators $T^a$ need to be defined. One possible choice is:

$$T^1 = \frac{1}{2}\begin{pmatrix}0 & 1\\ 1 & 0\end{pmatrix}, \quad T^2 = \frac{1}{2}\begin{pmatrix}0 & -i\\ i & 0\end{pmatrix}, \quad T^3 = \frac{1}{2}\begin{pmatrix}1 & 0\\ 0 & -1\end{pmatrix}, \tag{2.26}$$

that satisfy the commutation relation

$$[T^a, T^b] = \epsilon_{abc}T^c. \tag{2.27}$$

These are the *weak isospin* operators. The weak isospin is the charge of the weak interactions, in the same way the electric charge is the charge of the QED, telling how the particles interact. Using these gives the covariant derivative as

$$D_\mu = \partial_\mu \mathbb{1} + igW_\mu^i T_i = \partial_\mu \mathbb{1} + \frac{ig}{2}\begin{pmatrix} W^3 & (W^1 - iW^2) \\ (W^1 + iW^2) & -W^3 \end{pmatrix}. \tag{2.28}$$

This describes the charged weak interaction in the off-diagonal terms. However the diagonal terms are not yet complete as it turns out the physical particles related to the neutral weak interaction are a linear combination of the neutral $W_\mu^3$ gauge field and another neutral field $B_\mu$. The missing field comes from the U(1) symmetry of the Lagrangian. This combination of symmetry groups turns out to include electric interactions.

The remaining U(1) symmetry can be included by simply performing an SU(2)×U(1) transformation instead of the SU(2) one shown above. Taking the transformation to be of the form

$$\mathbf{U} = e^{i\omega^a T_a} e^{iY\alpha} \tag{2.29}$$

where Y is the charge coupled to the U(1) interaction, to be specified later. Allowing $\omega_a$ and $\alpha$ to depend on $x$, the free Lagrangian becomes:

$$\begin{aligned} \mathcal{L} \to \mathcal{L}' &= \bar{\psi} U^\dagger(x)(i\partial\!\!\!/ - m)U(x)\psi \\ &= \bar{\psi}(i\partial\!\!\!/ - m)\psi + i\omega^a \bar{\psi}(\partial\!\!\!/ T_a(x))\psi + iY\bar{\psi}(\partial\!\!\!/\alpha(x))\psi \end{aligned} \tag{2.30}$$

To counter the excessive terms, the covariant derivative is defined as

$$D_\mu = \partial_\mu + igW_\mu + ig'YB_\mu, \tag{2.31}$$

where $g$ and $g'$ are coupling constants and the gauge fields transform as

$$W_\mu \to W'_\mu = e^{i\omega^a T_a(x)} W_\mu e^{-i\omega^a T_a(x)} + \frac{i}{g}(\partial_\mu e^{i\omega^a T_a(x)}) e^{-i\omega^a T_a(x)}, \quad B_\mu \to B'_\mu = B_\mu + \frac{iY}{g'}\partial_\mu \alpha(x). \tag{2.32}$$

The Lagrangian written with the covariant derivative is

$$\mathcal{L} = \bar{\psi}(i\partial\!\!\!/ - m)\psi + ig\bar{\psi}\gamma^\mu W_\mu^a T_a \psi + ig'\bar{\psi}\gamma^\mu Y B_\mu \psi \tag{2.33}$$

and the covariant derivative written explicitly, using the same generators as above

$$
\begin{aligned}
D_\mu &= \partial_\mu \mathbb{1} + igW_\mu^a T_a + ig'YB_\mu \mathbb{1} \\
\Leftrightarrow D_\mu &= \begin{pmatrix} \partial_\mu + \frac{ig}{2}W_\mu^3 + ig'YB_\mu & \frac{ig}{2}(W_\mu^1 - iW_\mu^2) \\ \frac{ig}{2}(W_\mu^1 + iW_\mu^2) & \partial_\mu - \frac{ig}{2}W_\mu^3 + ig'YB_\mu \end{pmatrix}.
\end{aligned} \tag{2.34}
$$

This matrix describes the weak interactions. The off-diagonal terms cause the charged currents while the diagonal term contains the neutral current. Since the SU(2) part of the transformation affects only the left-handed fields, it is denoted as $\mathrm{SU}(2)_L$ and the U(1) transformation affecting both left- and right-handed fields couples to charge a $Y$ called the *weak hypercharge* of the fields. The symmetry group is denoted as $\mathrm{U}(1)_Y$. The weak hypercharge of an particle is defined as

$$
Q = T^3 + \frac{Y}{2} \leftrightarrow Y = 2(Q - T^3), \tag{2.35}
$$

where $Q$ is the electric charge and $T^3$ is the third component of weak isospin. This combined symmetry is then $\mathrm{SU}(2)_L \times \mathrm{U}(1)_Y$, and it is the unification of the electromagnetic interaction of the QED and the weak interaction into one electroweak interaction.

## 2.4 Spontaneous Symmetry Breaking and the Higgs boson

The inspiration for the symmetry breaking as the generator of masses of particles came from the study of superconductors in the 1950's by Bardeen, Cooper and Schrieffer [22]. It was by Nambu and Jona-Lasinio in 1961, that this idea was used to give masses to particles in a simplified model ( [23], [24]), and the application to Standard Model framework was done in 1964 separately by three different parties: Guralnik, Hagen and Kibble [25], Brout and Englert [26] and Higgs [27]. This mechanism is often cited as the Higgs mechanism for compactness, but a more just name for it is Englert-Brout-Higgs-Guralnik-Hagen-Kibble mechanism. The theoretical work and the hunt for the Higgs particle inspired by it culminated in the finding of the Higgs boson and the recognition for Englert and Higgs, who got a Nobel prize in 2013, almost half a century after the invention of the mechanism [28].

In spontaneous symmetry breaking, the Lagrangian itself is invariant under the symmetry, but the ground state of the system is not. The symmetry of the Lagrangian is required for renormalizable theories and this way the masses of the bosons can be generated without losing that property. Concretely, for gauge theories like SU(2) this means that for the ground state denoted as $|0\rangle$:

$$e^{i\omega_a T^a} |0\rangle \neq |0\rangle \,. \tag{2.36}$$

So while the initial state of the system is described by the Lagrangian that satisfies $e^{i\omega_a T^a}\mathcal{L} = \mathcal{L}$ i.e. it is symmetrical, the ground state that the system will evolve into no longer has this property and the symmetry is said to be spontaneously broken. The Goldstone theorem states that breaking of an exact and continuous global symmetry gives rise to a massless scalar particle called the Goldstone boson [29]. It is these Goldstone particles that will become the mass degrees of freedom for gauge bosons we derived above for the $\mathrm{SU}(2)_L \times \mathrm{U}(1)_Y$ symmetry group. The Goldstone bosons are said to be eaten by the gauge bosons. Now the symmetry will be broken as

$$\mathrm{SU}(2)_L \times \mathrm{U}(1)_Y \rightarrow \mathrm{U}(1)_{em} \tag{2.37}$$

which is to say that there is still some U(1) symmetry left that will leave the photons massless. The numbers of generators for the symmetry group before and after the symmetry breaking gives the number of broken symmetries. For $\mathrm{SU}(2)_L \times \mathrm{U}(1)_Y$ there are three $T^a$ and an $\alpha$ as the generators. In $U(1)_{em}$ there is only one generator. This breaking will then correspond to three broken symmetries, giving birth to three Goldstone bosons.

A new field has to be added into the Lagrangian in order to achieve the SSB. Let the new scalar doublet be

$$\Phi \equiv \begin{pmatrix} \phi_0 \\ \phi^+ \end{pmatrix} \tag{2.38}$$

where both $\phi^+$ and $\phi_0$ are complex scalar fields. The terms added to the Lagrangian are

$$\mathcal{L}_{scalar} = \partial_\nu \Phi^\dagger \partial^\nu \Phi - V(\Phi^\dagger \Phi), \tag{2.39}$$

where the potential is of the form

$$V(\Phi^\dagger \Phi) = \mu^2 \Phi^\dagger \Phi + \lambda (\Phi^\dagger \Phi)^2. \tag{2.40}$$

The extrema of such potential can be found as

$$\frac{\partial V}{\partial \Phi^\dagger} = (\mu^2 + 2\lambda \Phi^\dagger \Phi)\Phi = 0. \tag{2.41}$$

The potential should be bounded from below in order to have a ground state for the system, which requires $\lambda > 0$. In case $\mu^2 > 0$, there is only one minimum in the potential

at $\Phi = 0$. If $\mu^2 < 0$, there are minima at $\Phi^\dagger\Phi = -\frac{\mu^2}{2\lambda}$ and a maximum at $\Phi = 0$. This is shown in the Figure (2.3).

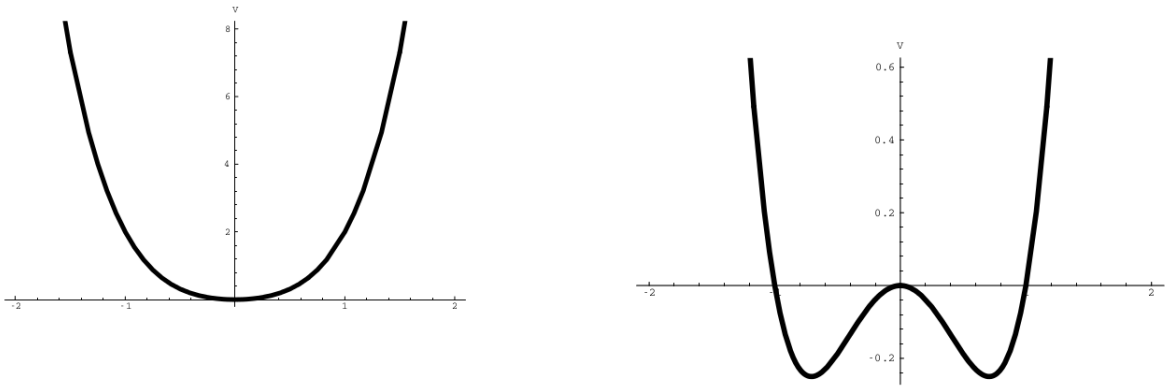


*(a)* *(b)*

Figure 2.3: Figure a) is the form of the potential when $\mu^2 > 0$, where there is only one minimum. In figure b) where $\mu^2 < 0$ there are multiple minima and a local maximum. [30].

The Lagrangian has to be symmetric before the SSB, and for that the partial derivative is replaced with the $SU(2)_L \times U(1)_Y$ covariant derivative:

$$\partial_\mu \Rightarrow D_\mu = \partial_\mu + igW_\mu + i\frac{g'}{2}B_\mu. \tag{2.42}$$

The fact that there are many possible minima that can be our ground state is a manifestation of the gauge freedom for the field $\Phi$. The gauge is selected by choosing a minimum to work with. Choosing to work in the so called unitary gauge, the would be massless Goldstone bosons do not appear, but instead mass terms for the bosons enter the Lagrangian. The unitary gauge means setting the doublet to

$$\begin{aligned} \Phi^\dagger\Phi = \phi^{+\dagger}\phi^+ + \phi_0^\dagger\phi_0 = -\frac{\mu^2}{2\lambda} \Rightarrow & \phi^+ = 0, \quad \phi_0 = \sqrt{-\frac{\mu^2}{2\lambda}} = v/\sqrt{2} \\ & \Leftrightarrow \Phi = \begin{pmatrix} v/\sqrt{2} \\ 0 \end{pmatrix} \end{aligned} \tag{2.43}$$

By choosing the gauge and thus attaching the ground state to one minimum around which to perturbate, the symmetry of the Lagrangian is lost, earning the name spontaneous symmetry breaking.

Defining new fields that are centered at the minimum

$$\phi_0' = \phi_0 - v/\sqrt{2}, \quad \phi^{+\prime} = \phi^+. \tag{2.44}$$

Perturbing around this minimum, the field is expanded as

$$\Phi = \begin{pmatrix} v/\sqrt{2} + H \\ 0 \end{pmatrix}. \tag{2.45}$$

Where $H << 1$ and it depends on the coordinates $H = H(x)$. There is still some symmetry left, as this field is invariant under the $SU(2)_L \times U(1)_Y$ transformations of the form

$$\mathbf{U} = e^{-i\frac{\theta}{2}} \begin{pmatrix} e^{i\frac{\theta}{2}} & 0 \\ 0 & e^{-i\frac{\theta}{2}} \end{pmatrix} = \begin{pmatrix} 1 & 0 \\ 0 & e^{-i\theta} \end{pmatrix}, \quad \mathbf{U}\Phi = \Phi. \tag{2.46}$$

Matrices of this type belong to a representation of $U(1)$ and this remaining symmetry keeps the photon massless. Using this field $\Phi$ that has a hypercharge of $Y = 1/2$ and the covariant derivative $D_\mu$ from (2.35), the first term $(D_\mu\Phi)^\dagger D^\mu\Phi = |D_\mu\Phi|^2$ of the Lagrangian becomes

$$\begin{aligned} D^\mu\Phi = &\left[ \begin{pmatrix} \partial_\mu + \frac{i}{2}\left(gW_\mu^3 + g'B_\mu\right) & \frac{ig}{2}\left(W_\mu^1 - iW_\mu^2\right) \\ \frac{ig}{2}\left(W_\mu^1 + iW_\mu^2\right) & \partial_\mu + \frac{i}{2}\left(-gW_\mu^3 + g'B_\mu\right) \end{pmatrix} \begin{pmatrix} v/\sqrt{2} + H \\ 0 \end{pmatrix} \right] \\ \Rightarrow |D^\mu\Phi|^2 = &\partial_\mu H \partial^\mu H + \frac{g^2}{4}\left(W_\mu^1 + iW_\mu^2\right)\left(W^{1\mu} - iW^{2\mu}\right)\left(v/\sqrt{2} + H\right)^2 \\ &+ \frac{1}{4}\left(gW_\mu^3 - g'B_\mu\right)^2\left(v/\sqrt{2} + H\right)^2 \end{aligned} \tag{2.47}$$

Equation (2.58) show that the gauge fields mix, $W^1$ with $W^2$ and $W^3$ with $B$. The physical gauge bosons after the SSB are then superpositions of the mixed fields.

The superpositions $\left(W_\mu^1 \mp iW_\mu^2\right)$ are the charged currents of the theory. The physical boson that carries a charge is denoted

$$W_\mu^\pm = \frac{\left(W_\mu^1 \mp iW_\mu^2\right)}{\sqrt{2}}. \tag{2.48}$$

The two remaining fields are responsible for the neutral current of the weak interaction. The physical boson is denoted as

$$\sqrt{g^2+g'^2}Z_\mu^0 = gW_\mu^3 - g'B_\mu, \tag{2.49}$$

where the factor in front of $Z_\mu^0$ has been chosen for normalization. The orthogonal linear combination to this will be the last physical gauge boson, the photon $A_\mu$:

$$\sqrt{g^2+g'^2}A_\mu = g'W_\mu^3 + gB_\mu. \tag{2.50}$$

It is customary to use the *Weinberg angle* $\theta_W$ instead of the couplings as

$$\sin\theta_W = \frac{g'}{\sqrt{g^2+g'^2}}, \tag{2.51}$$

and rewrite the definitions as

$$\begin{aligned} Z_\mu^0 =& W_\mu^3\cos\theta_W - B_\mu\sin\theta_W \\ A_\mu =& W_\mu^3\sin\theta_W + B_\mu\cos\theta_W. \end{aligned} \tag{2.52}$$

Inverting these relations gives the original gauge fields in terms of $A_\mu$ and $Z_\mu^0$ as

$$\begin{aligned} W_\mu^3 =& A_\mu\sin\theta_W + Z_\mu^0\cos\theta_W \\ B_\mu =& A_\mu\cos\theta_W - Z_\mu^0\sin\theta_W, \end{aligned} \tag{2.53}$$

One final relation can be found using the knowledge of photon coupling strength $-e$, giving the result

$$e = \frac{1}{2}\left(g\sin\theta_W + g'\cos\theta_W\right) = \frac{gg'}{\sqrt{g^2+g'^2}}, \tag{2.54}$$

allowing the new coupling constants to be written in terms of one unknown, the Weinberg mixing angle

$$g = \frac{e}{\sin\theta_W}, \quad g' = \frac{e}{\cos\theta_W}. \tag{2.55}$$

The value of this mixing angle $\theta_W$ is something the Standard Model framework does not explain but it has been measured to be around $\theta_W \simeq 23°$.

Using these new definitions for the physical gauge bosons, the covariant derivative term of the Higgs field becomes

$$
\begin{aligned}
|D_\mu \Phi|^2 =& \partial_\mu H \partial^\mu H + \frac{e^2}{2\sin^2\theta_W} W_\mu^- W^{+\mu} \left(v/\sqrt{2} + H\right)^2 \\
&+ \frac{1}{4}\frac{e^2}{\sin^2\theta_W \cos^2\theta_W} Z_\mu^0 Z^{0\mu} \left(v/\sqrt{2} + H\right)^2
\end{aligned}
\tag{2.56}
$$

Expanding $(v/\sqrt{2} + H)^2 = v^2/2 + \sqrt{2}vH + H^2$ and inserting this back to the full scalar Lagrangian (2.49) gives an equation where the mass terms of the bosons are visible:

$$
\begin{aligned}
\mathcal{L}_{scalar} =& \partial_\mu H \partial^\mu H + \frac{e^2 v^2}{4\sin^2\theta_W} W_\mu^- W^{+\mu} + \frac{1}{8}\frac{e^2 v^2}{\sin^2\theta_W \cos^2\theta_W} Z_\mu Z^\mu + 0 A_\mu A_0^\mu + 2\mu^2 H^2 \\
&+ \frac{e^2}{2\sin^2\theta_W} \left(\sqrt{2} v W_\mu^- W^{+\mu} H + W_\mu^- W^{+\mu} H^2\right) + \frac{1}{4}\frac{e^2}{\sin^2\theta_W \cos^2\theta_W} \left(\sqrt{2} v Z_\mu Z^\mu H + Z_\mu Z^\mu H^2\right) \\
&+ \frac{\mu^2 v^2}{4} \left(\frac{4}{v^3} H^3 + \frac{1}{v^4} H^4 - 1\right),
\end{aligned}
\tag{2.57}
$$

where the dynamic term of the field $H$ and the mass terms for all the bosons are on the first row and the interactions between the massive bosons with each other on the second row. The third row contains the self-interactions of the Higgs boson. It shows that all the bosons except $A_\mu$ got a quadratic mass term and interact with the new field $H$. The photon field $A_\mu$ should indeed remain massless for the QED phenomenology to hold. This is the core of the Standard Model of electroweak symmetry breaking. The model is also known as the Weinberg-Salam-Glashow -model as Glashow's work [31] was developed further independently by Weinberg [32] and Salam [33], resulting in the model of the weak and electric interactions with four massive and one massless gauge bosons.

Some aspects of this Lagrangian worth pointing out are that the masses of the gauge bosons of the weak interaction are related by

$$
m_W = \frac{ev}{2\sin\theta_W}, \quad m_Z = \frac{ev}{4\sin\theta_W \cos\theta_W} \quad \Leftrightarrow \frac{m_W}{m_Z} = 2\cos\theta_W, \tag{2.58}
$$

so a measurement of the Weinberg mixing angle $\theta_W$, combined with the knowledge about the vacuum energy and elementary charge completely fix the masses of $W^\pm$ and $Z^0$. Reversing this, it can be seen that knowing the masses of $W^\pm$ and $Z^0$ and measuring the mixing angle, will give the vacuum expectation value of the Higgs field, giving the coupling strengths of the Higgs boson with the other bosons. However the Higgs mass is something the Standard Model does not give a prediction about.

Earlier the Lagrangian for the leptons was presented with an explicit mass term $m^2\bar{\psi}\psi$. This is not entirely correct as such a mass term would cause right- and left-handed doublets

to mix and consequently violate the symmetry of the Lagrangian. However the Higgs doublet that was shown to give masses to the gauge bosons above can also be used to give the masses of the fermions in a way that conserves the symmetry through the SSB. It is done via introducing so called *Yukawa couplings* to the Lagrangian that are invariant under the symmetry group and are proportional to the expected value of the Higgs field. This leads to initially massless fermions that get their masses from the SSB of the symmetry group [34].

## 2.5 Quantum Chromodynamics

The success of non-Abelian gauge field theories in describing the weak interaction encouraged the use of similar approach in the formulation of the strong interaction. Strong interaction is responsible for interactions of the quarks with each other, resulting in bound states such as the baryons like the proton that consists of three quarks, and the mesons such as $\pi^+$ consisting of a quark and an antiquark. Maybe the most striking difference between the strong interaction and the electroweak interaction is the coupling strength. As the name might suggest, the coupling between the interactions of the quarks is strong compared to weak or electric couplings in the low energy regions. This leads to divergences when calculating the theory using perturbations. However the coupling strengths in all of the interactions are not constants but variables with respect to energy of the interaction. In the case of QCD, the coupling strength gets smaller as the energy increases, so that there exists a perturbative QCD region at high energies. The division of perturbative and non-perturbative QCD is around the energy scale $\lambda_{QCD} \approx 200$ MeV.

In analogy with the QED, the theory describing these interactions is known as the Quantum Chromodynamics (QCD), where *chromo* references to colour, which is the charge of the strong interaction. It should be stated that this has no connection to the visual colours of everyday life, but it is just a lively name for another quantum number.

There are three different colour charges available to the quarks, labelled as red(r), green(g) and blue(b), and the antiparticles will carry the antiversions of the colours namely antired($\bar{\text{r}}$), antigreen($\bar{\text{g}}$) and antiblue ($\bar{\text{b}}$). However these colours have never been observed directly, as we are not able to detect a single quark on its own. We only observe combinations of quarks so that the sum of the constituent colours will be colorless i.e. a combination of equal parts of all the colours or a sum of colours and their anticolours in equal amounts. This is called the *colour confinement* of the quarks.

There are six quarks in the SM: up, down, charm, strange, top and bottom. Each quark is a spin-$\frac{1}{2}$ particle that can be described by a four-component Dirac spinor. On top of that the quarks are colour triplets with respect to $\mathrm{SU}(3)_C$ group transformations, where $C$ refers to the colour charge. For example the up and down quarks:

$$u = \begin{pmatrix} u_r \\ u_g \\ u_b \end{pmatrix}, \quad d = \begin{pmatrix} d_r \\ d_g \\ d_b \end{pmatrix}. \tag{2.59}$$

With the same approach as with the QED and weak interactions, the free Lagrangian of the particle content (six fermions and their antiparticles) is used to find a global gauge invariance that is promoted into a local one, introducing gauge fields to maintain invariance. The free Lagrangian

$$\mathcal{L}_{free} = \sum_{f=1}^{6} [\bar{\mathbf{q}}_f (i\gamma^\mu \partial_\mu - m_f)\mathbf{q}_f] \tag{2.60}$$

The Lagrangian is invariant with respect to global SU(3) transformations as the fields transform

$$\mathbf{q} \Rightarrow \mathbf{q}' = \mathbf{U}\mathbf{q}, \quad \bar{\mathbf{q}} \Rightarrow \bar{\mathbf{q}} = \mathbf{U}^\dagger \bar{\mathbf{q}}. \tag{2.61}$$

Promoting this invariance to a local one $\mathbf{U} \Rightarrow \mathbf{U}(x)$ requires the use of covariant derivative in order to conserve the invariance

$$\partial_\mu \Rightarrow D_\mu = \partial_\mu + i g_S \mathbf{G}_\mu \tag{2.62}$$

where the new gauge field $\mathbf{G}_\mu$ transforms under $\mathrm{SU}(3)_C$ as

$$\mathbf{G}_\mu \Rightarrow \mathbf{G}'_\mu = \mathbf{U}\mathbf{G}_\mu\mathbf{U}^\dagger + \frac{i}{g_S}(\partial_\mu \mathbf{U})\mathbf{U}^\dagger. \tag{2.63}$$

Here $\mathbf{G}_\mu$ is a 3x3 hermitian and traceless matrix describing the gauge field and $g_S$ is the coupling strength of the strong interaction. The set of these matrices in $\mathrm{SU}(3)_C$ can be written in terms of the basis of eight Gell-Mann matrices as

$$\mathbf{G}_\mu = \frac{1}{2}\sum_{i=1}^{8} \lambda_a G^a_\mu \tag{2.64}$$

where $G^a_\mu$ are real coefficients and the Gell-Mann matrices are explicitly

$$\lambda_1 = \begin{pmatrix} 0 & 1 & 0 \\ 1 & 0 & 0 \\ 0 & 0 & 0 \end{pmatrix}, \quad \lambda_2 = \begin{pmatrix} 0 & -i & 0 \\ i & 0 & 0 \\ 0 & 0 & 0 \end{pmatrix}, \quad \lambda_3 = \begin{pmatrix} 1 & 0 & 0 \\ 0 & -1 & 0 \\ 0 & 0 & 0 \end{pmatrix},$$
$$\lambda_4 = \begin{pmatrix} 0 & 0 & 1 \\ 0 & 0 & 0 \\ 1 & 0 & 0 \end{pmatrix}, \quad \lambda_5 = \begin{pmatrix} 0 & 0 & -i \\ 0 & 0 & 0 \\ i & 0 & 0 \end{pmatrix}, \quad \lambda_6 = \begin{pmatrix} 0 & 0 & 0 \\ 0 & 0 & 1 \\ 0 & 1 & 0 \end{pmatrix}, \tag{2.65}$$
$$\lambda_7 = \begin{pmatrix} 0 & 0 & 0 \\ 0 & 0 & -i \\ 0 & i & 0 \end{pmatrix}, \quad \lambda_8 = \frac{1}{\sqrt{3}} \begin{pmatrix} 1 & 0 & 0 \\ 0 & 1 & 0 \\ 0 & 0 & -2 \end{pmatrix}.$$

For the full QCD Lagrangian, the dynamical term for the new boson field $\mathbf{G}_\mu$ that contains the gluons is needed. It can be written the usual way of the non-Abelian theories by using the Yang-Mills construction

$$\mathbf{G}_{\mu\nu} = \partial_\mu \mathbf{G}_\nu - \partial_\nu \mathbf{G}_\mu + i g_S (\mathbf{G}_\mu \mathbf{G}_\nu - \mathbf{G}_\nu \mathbf{G}_\mu). \tag{2.66}$$

The dynamical term for gluons is

$$\begin{aligned} \mathcal{L}_{gluon} &= -\frac{1}{4} \sum_{a=1}^{8} G^a_{\mu\nu} G^{\mu\nu}_a \\ &= -\frac{1}{4} (\partial_\mu G^a_\nu - \partial_\nu G^a_\mu)(\partial^\mu G^\nu_a - \partial^\nu G^\mu_a) - \frac{1}{4} g_S^2 f^{abc} f_{ade} G^\mu_b G^\nu_c G^d_\mu G^e_\nu \\ &\quad + \frac{1}{2} f_{abc} (\partial_\mu G^a_\nu - \partial_\nu G^a_\mu) G^{\mu b} G^{\nu c} \end{aligned} \tag{2.67}$$

where $G^a_{\mu\nu}$ are the coefficients of the matrix $G_{\mu\nu}$ expanded in the basis of $\lambda_a$. The summation is implied through repeated indices $a$, $b$ and $c$ according to the Einstein summation convention and the explicit summation signs were removed. The constants $f^{abc}$ are the structure constants of the $\mathrm{SU}(3)_C$ defined by the commutation relation

$$\begin{aligned} [\lambda_a, \lambda_b] = \lambda_a \lambda_b - \lambda_b \lambda_a &= 2i \sum_{c=1}^{8} f_{abc} \lambda_c \\ f_{123} = 1, \quad f_{458} = f_{678} &= \frac{\sqrt{3}}{2} \\ f_{147} = f_{246} = f_{257} = f_{345} = f_{516} = f_{637} &= \frac{1}{2}. \end{aligned} \tag{2.68}$$

Combining the covariant derivative $D_\mu$ and the gluon term with the free Lagrangian, we get the full QCD Lagrangian with the interactions of quarks and the gluon self-interactions as

$$\begin{aligned}\mathcal{L}_{QCD} = &\sum_{f=1}^{6}[\bar{\mathbf{q}}_f(i\gamma^\mu\partial_\mu - m_f)\mathbf{q}_f] - \frac{1}{4}(\partial_\mu G^a_\nu - \partial_\nu G^a_\mu)(\partial^\mu G^\nu_a - \partial^\nu G^\mu_a) \\ &- \sum_{f=1}^{6}[g_s\bar{\mathbf{q}}_f\gamma^\mu\mathbf{G}_\mu\mathbf{q}_f] - \frac{1}{4}g_S^2 f^{abc}f_{ade}G^\mu_b G^\nu_c G^d_\mu G^e_\nu + \frac{1}{2}f_{abc}(\partial_\mu G^a_\nu - \partial_\nu G^a_\mu)G^{\mu b}G^{\nu c},\end{aligned} \tag{2.69}$$

where the dynamic terms corresponding to propagators of the fermion and gluon fields are on the first row and the interaction terms for the quarks and the gluon self-interaction are on the second row.

The problem of perturbation theory being non-applicable since coupling is too strong is ameliorated by the ultraviolet behaviour of the strong interaction first found by by D. Politzer [35], D. Gross and F. Wilczek [36]. In the high energy regime, the coupling strength of the strong interaction grows weaker, allowing the perturbation theory to make sense again. This is known as the *asymptotic freedom* of the QCD. However there are also other ways of treating the theory if one wants to calculate in the low energy regimes, one of the most prominent being the lattice QCD, where the phase-space is constructed from discrete set of points where the path integrals of the quantum fields are calculated can be calculated in a way that avoids the divergences. More on the lattice formulation of QCD can be found from [37].

The property of colour confinement in the QCD is the cause of hadronic jets in hadron collider experiments that will be discussed about in the second part of this thesis. As the quarks inside colliding hadrons exchange gluons and get knocked away from their colour neutral environment, new quarks are created from the vacuum in order to uphold the colour neutrality. This is called the *hadronisation* of the quarks and it is seen as cascades of hadrons collimated into jets in particle detectors where the particle collisions take place. This is a profound difference between the strong interaction and the other interactions described as there is no similar concept of confinement with weak or electric charges.

The quark masses and participation in weak interactions can be done similarly as was done with the leptons. The quarks form doublets and singlets of up and down type quarks depending on their handedness. For example, the first generation of quarks is

$$q^L_1 = \begin{pmatrix} u^L \\ d^L \end{pmatrix}, \quad u^R, \quad d^R, \tag{2.70}$$

so that the left-handed fields again participate in the weak interaction and both right- and left-handed fields participate in the electric interactions and neutral weak interactions.

This overview of the QCD concludes the review of the core of the Standard Model of particle physics. The Standard Model Lagrangian will contain the Lagrangians presented here, namely the QCD, electroweak and the Higgs Lagrangians and it will be invariant under the symmetry group $\mathrm{SU}(3)_C \times \mathrm{SU}(2)_L \times \mathrm{U}(1)_Y$. The mass terms for bosons will be generated by the SSB of the Higgs doublet, resulting in three of the four degrees of freedom of the Higgs doublet being absorbed by the gauge bosons $W^{\pm}$ and $Z^0$. The final degree of freedom appears as a particle that interacts with the massive particles of the theory, known as the Higgs boson. The quarks and charged leptons attain masses by addition of the Yukawa potentials, that lead to the particles interacting with the Higgs boson, resulting in mass terms.

The goal of this chapter was to show how the concept of symmetry produced remarkable results with the interactions and their mediating gauge bosons being introduced to the theory almost as if by accident. As was in the case of neutral weak currents mediated by the $Z^0$ boson, the prediction of such a gauge particle came long before the experiments managed to confirm it. With such astonishing results it is no wonder that the particle physicists have stuck with deciphering Nature through its symmetries for so long. This theme of symmetries will continue as a way of extending the Standard Model is presented in the next chapter, but first the need for such extensions as a remedy for some more problematic aspects of the Standard Model has to be discussed.

## 2.6 Problems of the Standard Model

Even though the Standard Model of particle physics can unarguably be called as one of the greatest achievements of theoretical and experimental physics, it has its shortcomings. There are things that the SM does not explain like the neutrino masses that are known to exist due to the observation of neutrino oscillations [38]. This startling observation was awarded the Nobel prize of Physics in 2015 [39]. Another example is the baryon asymmetry i.e. why is there so much matter but so little antimatter in the Universe [40]. The Standard Model does not give any clues about dark matter either, one of the largest open problems of cosmology today [41].

There are also theoretically questionable features of the SM, for example the large number of free parameters: the coupling strengths of the gauge bosons, the masses of quarks and leptons and so on. In total there are 19 free parameters to be determined. There is the so called Hierarchy problem revolving around the mass of the Higgs boson. It is expected to get very large contributions to its mass from quantum loop corrections in higher order quantum field theory calculations, but somehow these seem to cancel and the Higgs mass is the observed, relatively low 125 $\mathrm{GeV/c^2}$. One also has to mention that obviously the

SM does not say anything about gravity, since it would certainly be good to take all the known interactions to account in our theories. This however is not the most immediate problem in the horizon, but it is good to keep in mind that it would be pleasant to have at least some indication of how to extend the theory to include gravitational effects.

These are the problems that have been in the works after the 1970's when the SM was completed theoretically. There have been many different areas of research trying to find the theory that explains as much as the SM but also solves some of the aforementioned problems and inconveniences, like string theory, higher order symmetry groups SU(5) and SU(10) and supersymmetric theories. It is the latter that will be presented in more detail in the rest of this theory section.

# Chapter 3

# Supersymmetry

## 3.1 A new symmetry of space-time

The quest for symmetries did not stop at the completion of the Standard Model, as formulating physics by through symmetry had proven to be a valuable tool. It was shown by Coleman and Mendula in 1969 that addition of new space-time symmetries to the Standard Model symmetry group would violate the relativistic quantum field theoretical grounds of the model [42]. This restriction could be circumvented by the use of *supersymmetric algebra* in defining the symmetry groups, leading to a new unique type of space-time symmetry. The difference to the algebra used in defining the regular symmetry groups is that instead of only commutator relations, also anticommutators are used in supersymmetric algebras. The symmetry groups based on the supersymmetric algebras are called *graded Lie groups* instead of the regular *Lie groups*.

This new symmetry adds degrees of freedom to the usual four-dimensional concept of space-time, extending space-time into a *superspace*. These added dimensions relate to the ordinary four dimensions through supersymmetry transformations. It has a profound effect on the particles that are formulated as excitations of the *superfields* spanning this new space-time as the supersymmetric transformations relate bosonic and fermionic degrees of freedom together. This is to be interpreted as the bosons and fermions being just two states of the particles, differing by spin-1/2 [43]. It is however clear that this symmetry has to be broken somehow, as unbroken symmetry would require there to be a boson for every fermion with the same mass, which has not been observed. Breaking the symmetry can be used to push the masses of the supersymmetric partners to higher energies.

The foundations of supersymmetry as a space-time symmetry in terms of quantum field theory were created in the 1970's by various physicists independently. At least three parties are usually credited with the discovery: Gervais & Sakita [44], Golfand & Likhtman [45] and Volkov & Akulov [46]. Fayet [47] later proposed the Minimal Supersymmetric extension to the Standard Model (MSSM), which suggested a solution to the hierarchy problem combining the supersymmetric ideas to particle physics.

The hierarchy problem comes from radiative corrections to the Higgs mass. These corrections to the Higgs mass require an enormous fine tuning in order to get the theoretical value to match the observed value. At one loop level there are two corrections to the Higgs self-energy i.e. its mass. There is the self-interaction loop in Figure 3.1 a) and the

fermion loop in Figure 3.1 b).

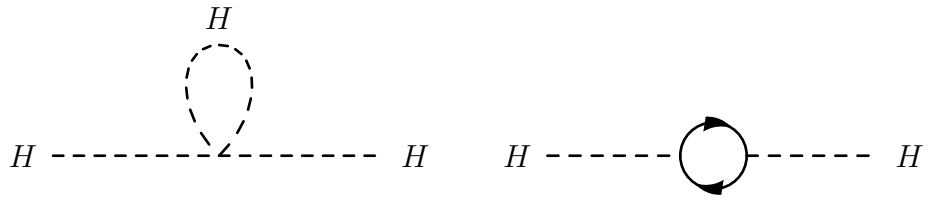


Figure 3.1: The one loop corrections to Higgs boson mass. On the left the Higgs self-interaction and on the right the fermion loop interaction

Using the Feynman rules for the diagrams, the contributions of these correcting terms can be found to be of the form

$$\lambda \int^{\Lambda} \frac{d^4k}{k^2 - M_H^2} \sim \lambda \Lambda^2 \phi^\dagger \phi, \quad g_f^2 \int^{\Lambda} \frac{d^4k}{\not{k}\not{k}} \sim -g_f^2 \Lambda^2 \phi^\dagger \phi. \tag{3.1}$$

where $\lambda$ is the Higgs coupling strength to itself and $g_f$ is the Higgs coupling strength to fermions. The negative sign of the latter term is due to the fermionic nature of the loop diagram. So the two contributions are giving opposite contributions to the Higgs boson mass. The symbol $\Lambda$ is known as the cut-off scale of the theory. It tells us at what point our theory is no longer applicable since the physical effects that are not included to the theory start appearing and causing changes to the observables. For Standard Model this scale can be set at the energies where the effects of gravity cannot be neglected anymore. This quantum gravity is expected to appear around the Planck mass energies

$$M_P = (G_N)^{-\frac{1}{2}} \simeq 1.2 \times 10^{19} \text{GeV}. \tag{3.2}$$

However if there appears new physics before those energies, such as new particles that come from theories beyond the Standard Model, this cut-off energy has to be set lower than that energy scale.

The mass term for the Higgs boson from the electroweak symmetry breaking was $M_H \phi^\dagger \phi$, where $M_H = \sqrt{2}\mu$. When calculating the total correction to the mass of the particle, one has to sum all the terms together with their relative signs. This mass term with the corrections will be of the form

$$M'_H \phi^\dagger \phi \simeq \mu'^2 \phi^\dagger \phi = [\sqrt{2}\mu + (\lambda - g_f^2)\Lambda^2] \phi^\dagger \phi \tag{3.3}$$

Now it can be seen that if the Higgs self-coupling and the fermionic coupling strengths differ even a little bit, the effect on the Higgs boson mass can be enormous as it is weighted by the square of the energy scale for new physics $\Lambda$. Since the Standard Model did not give a prediction of the Higgs mass, this situation can be remedied by setting $\mu$ to compensate this correction, so that the observed Higgs mass is $M_{\mathrm{H}} = 125$ GeV/c$^2$. It is however exactly this fine-tuning that is called the Hierarchy problem, as it seems kind of sketchy for the Higgs mass to be tuned so low, if the correction term is of the order of $10^{28}$ GeV/c$^2$, at least when there is no reason to expect $\mu$ to be so large.

This inconvenience is mended if a symmetry relates sets the fermionic and bosonic self-couplings to equality as exactly $\lambda = g_f^2$, removing the term containing $\Lambda^2$. One symmetry that does just this is the supersymmetry. It will require every fermion and boson of the Standard Model to be related to a supersymmetric boson and a supersymmetric fermion respectively. This forces the theory to have twice the particle content.

As the supersymmetric particles have not been observed, they must be more massive than the current masses studied by collider experiments. This can indicated by breaking the supersymmetry. On the other hand this kind of fine tuning was just what one tried to get rid of in the first place with the hierarchy problem. This is however many orders of magnitude less fine tuning than originally, if the supersymmetric particles are around the energy scale of $\sim 1$ TeV. This requirement is set by the terms arising from breaking of the supersymmetry [48]. In this energy scale, the lightest supersymmetric partner is expected to be seen at the LHC Run 2 at 14 TeV collision energies [49].

Even though this seems like a stretch to fix the original problems of the Standard Model with so much more complications, there are other aspects making supersymmetry interesting. In order to preserve baryon and lepton number conservation that has been observed to hold very accurately, so called R-parity conservation is imposed on many models. The SM particles all have R-parity $+1$ and the supersymmetric particles have R-parity of $-1$. One consequence of this conservation law is that the lightest supersymmetric particle cannot decay, as there is no way for the R-parity to be conserved as it could only decay to lighter, the SM particles. This makes it a candidate for the dark matter that can be observed only through gravity, as the SM does not contain a particle able to match the dark matter observations.

Another feature of supersymmetry is that the new supersymmetric particles at higher energy scales allows the running coupling constants of the Standard Model become unified at a certain energy scale. This reduces the number of free parameters of the SM, since it unifies all interaction to just one interaction that manifests as three different interactions at low energies when the symmetry is broken.

## 3.2 Two Higgs-doublet models

In supersymmetric theories the particles will be distinguished by their chirality. This sets the up- and down-type quarks in an unequal position when bestowing masses to them through the Yukawa coupling with the Higgs boson doublet. The Higgs doublet can generate masses only to up-type or down-type quarks but not both at the same time. However as was done with the SM, one can add another complex scalar field to give masses to all the quarks. This kind of models are called two Higgs-doublet models (2HDM) and they offer a large variety of appealing properties that come with the added freedom from the parameters related to the second Higgs-doublet, making 2HDM a popular field of study as the Standard Model extensions.

In the most general form the scalar potential contains 14 parameters and it can have minima that are CP-conserving, CP-violating and charge violating. For example baryon asymmetry can be brought to the model using this potential. There are also difficulties, most prominent of which is the possibility for Flavour Changing Neutral Currents (FCNC) at the tree-level of the theory. In the SM these occur at higher orders and a tree-level FCNC has not been observed. These currents can be suppressed by with additional symmetries.

A common feature of in the 2HDM is the existence of additional Higgs bosons. With the added doublet, there are in total eight degrees of freedom for the Higgs fields. Three of these are used by the $W^{\pm}$ and $Z^0$ in order to aquire mass. The five remaining fields are physical Higgs bosons: Two neutral scalars, two charged scalars and one pseudoscalar [50]. The ratio of the vacuum expectation values of the two Higgs-doublets determines the interactions between the Higgs' and other particles in a similar manner as in the SM case. This makes the parameter

$$\tan\beta = \frac{v_2}{v_1} \tag{3.4}$$

highly interesting to the phenomenology of the two Higgs-doublet models.

### 3.2.1 The Higgs sector in minimal supersymmetric models

In the Minimal Supersymmetric Standard Model (MSSM) extension of the SM, there are additional constraints set upon the general 2HDM scalar potential. The scalar potential should break $SU(2)_L \times U_Y$ symmetry while preserving $U(1)_{QED}$. It should also be CP-conserving at tree-level and bounded from below. The supersymmetry has to be broken as the superpartners do not have same masses, and in MSSM this has to be done in a certain way called the soft-SUSY breaking. It is required that the soft-SUSY breaking masses of the Higgs fields are not equal $m_{H_1} \neq m_{H_2}$. Using these constraints, the number of free

parameters is reduced and a phenomenologically more feasible model than the general 2HDM is created [51]. The two free parameters are usually set to be the ratio of the vacuum expectation values of the two scalar doublets and the mass of the pseudoscalar Higgs boson:

$$\tan\beta, \qquad M_A. \tag{3.5}$$

The masses of the Higgs bosons satisfy

$$\begin{aligned} M_{\mathrm{H}} &> \max\left(M_{\mathrm{A}}, M_{\mathrm{Z}}\right) \\ M_{\mathrm{H}^{\pm}} &> M_{\mathrm{W}} \end{aligned}$$

which will cause the mass of the lightest Higgs boson $h$ to be

$$M_h \leq \min\left(M_{\mathrm{A}}, M_{\mathrm{Z}}\right) |\cos 2\beta| \leq M_{\mathrm{Z}}. \tag{3.6}$$

However as can be seen the lightest Higgs boson should have been found by now with $M_h \leq 91.1876$ GeV/c$^2$ from the LHC data, according to the MSSM tree level prediction. Nonetheless other SUSY theories can give predictions with higher masses for the lightest Higgs boson, that are yet to be excluded by experiments.

As there is only one scalar Higgs boson in the Standard Model, observing another Higgs boson in collider experiments would be a clear signal of the physics beyond the SM. The charged Higgs boson is one of the candidates that are being searched for. The coupling of the charged Higgs boson to leptons is relative to the mass of the lepton, so in the mass regime where the charged Higgs boson is expected, the favoured leptonic decay channel will be into $\tau$-lepton. The excess of these $\tau$-leptons with respect to the SM prediction is searched for in the data of CMS and ATLAS at CERN in order to find a sign of this new kind of a boson.

# Chapter 4

# Studying physics with collider experiments

In the following chapter some fundamental concepts for analysing particle collisions are presented. The properties of the proton that need to be accounted for in proton-proton collisions are discussed, and the coordinate system and useful quantities when detecting the collisions are introduced.

## 4.1 The coordinate system

The general coordinate system used in the CMS detector is right-handed with the $x$-axis pointing towards the center of the LHC ring, $y$-axis vertically upwards and $z$-axis in the counter clockwise direction along the beam pipe. The $x, y$-plane is called the transverse plane as the beams are perpendicular to it. The polar angle $\theta$ is measured as the deviation from the direction of the $z$-axis and the azimuthal angle $\phi$ is the deviation from the $x$-axis in the transverse plane. These coordinates are demonstrated in Figure 4.1.

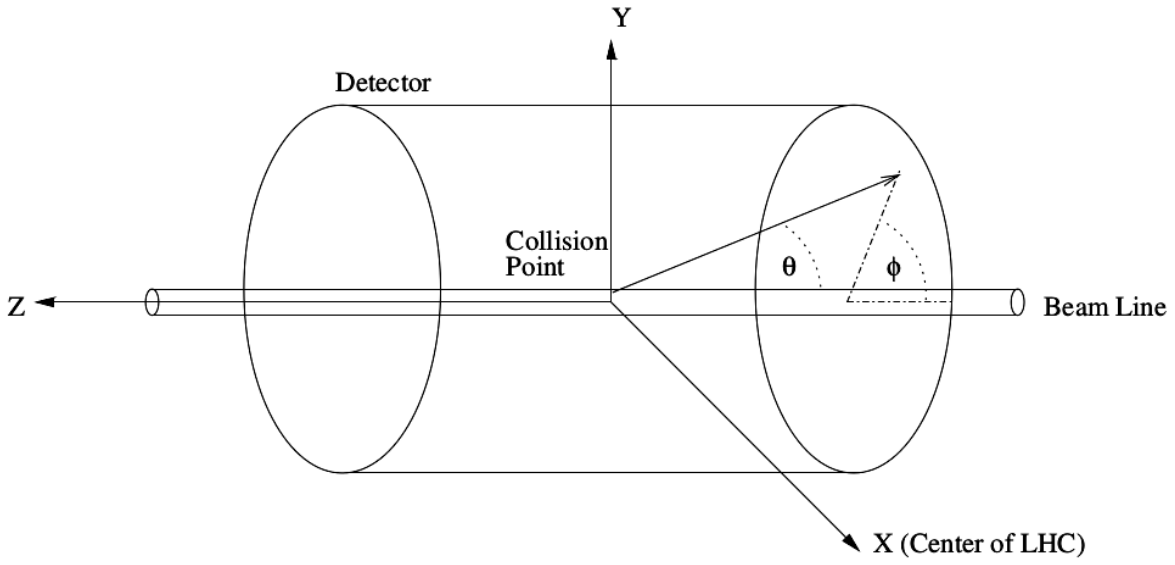


Figure 4.1: A schematic representation of the CMS coordinate system [52]

## 4.2 Useful quantities in collider experiments

Often used variable in describing the kinematics of particle collisions in accelerators is the *rapidity* $y$. Rapidity gives us a dimensionless quantity related to the velocity of the particle along the $z$-axis. It is defined in terms of energy of the particle $p_0$ and its longitudinal momentum i.e. the momentum along the $z$-axis $p_z$, as:

$$y = \frac{1}{2}\ln\frac{p_0 + p_z}{p_0 - p_z}. \tag{4.1}$$

The rapidity variable is dependent on the coordinate system we are in, but it has a very useful attribute with regard to Lorentz transformations: Rapidities are simply additive quantities in the relativistic region, unlike velocities. This makes moving from one frame of reference to another in terms of rapidity very easy. However, determining rapidity requires knowledge of two quantities of the particle, namely the energy and the longitudinal momentum. This is a luxury that is not easily achieved in particle physics experiments with nuclei and often a more convenient variable to determine is the *pseudorapidity* $\eta$.

Pseudorapidity describes the angle between the momentum $\boldsymbol{p}$ of the outgoing particle and the $z$-axis. It is defined by:

$$\eta = \frac{1}{2}\ln\frac{|\boldsymbol{p}| + p_z}{|\boldsymbol{p}| - p_z}. \tag{4.2}$$

When the particles are in the highly relativistic limit, as is often the case in particle accelerators, we have $m << |\boldsymbol{p}|$ and we can use the approximation $p_0 = \sqrt{m^2 + |\boldsymbol{p}|^2} \approx |\boldsymbol{p}|$. This approximation directly relates the rapidity and pseudorapidity variables together as:

$$\eta \approx y = \frac{1}{2}\ln\frac{p_0 + p_z}{p_0 - p_z}. \tag{4.3}$$

The relation between the angle $\theta$ and the pseudorapidity $\eta$ is:

$$\eta = -\ln[\tan(\frac{\theta}{2})]. \tag{4.4}$$

The reason for using pseudorapidity instead of the angle $\theta$ is the fact that the difference $\Delta\eta$ between two particles stays the same in any reference frame, unlike the angle $\theta$ that is changed by the Lorentz transformations.

With this in mind, the *angular distance* or separation between the tracks of two particles is defined as:

$$\Delta R = \sqrt{\Delta\eta^2 + \Delta\phi^2}. \tag{4.5}$$

Since both $\Delta\eta$ and $\Delta\phi$ are invariant to Lorentz boosts in the $z$-direction, the separation is the same in every frame of reference. This quantity $\Delta R$ is very useful when reconstructing the information about the collision from the decay products.

When determining which tracks came from the same interaction, the *transverse impact parameter* $\mathrm{IP_T}$ and *longitudinal impact parameter* $\mathrm{IP}_z$ are used. They describe the closest distance of a reconstructed particle track from the detector to the *primary vertex*, which is the point where the interaction took place. Respectively these distances are in the transverse and longitudinal directions.

Many of the particles created in collisions are not long-lived but decay quickly into other particles. The particles that decay inside the detector are called *unstable* and the particles that traverse the detector before decaying are called *stable*. When discussing decays, *branching ratio* $\mathcal{B}(A \to B)$ is the quantity describing what percentage of the particles A decay into particles B.

When searching for new particles, a quantity called the *transverse mass* $m_\mathrm{T}$ is often used as it is a Lorentz invariant. It can be used to reconstruct the mass of the particles from the observed transverse momenta of the decay products or in some cases, from the transverse momenta of a particle and missing transverse energy due to the other. Transverse mass in high energy physics is calculated as

$$m_\mathrm{T} = \sqrt{2p_{T_1}p_{T_2}\left(1 - \cos\theta\left(\vec{p}_{\mathrm{T}_1}, \vec{p}_{\mathrm{T}_2}\right)\right)} \tag{4.6}$$

where the particle masses are approximated to zero as the momentum is the dominant contribution to the total energies. Here $\theta$ is the angle between the momenta of the decay product particles. Particles are seen as Jacobian peaks in the transverse mass plots at $M/2$, where $M$ is the mass of the particle. If a statistically significant peak appears at a mass where there is no known particle, a new particle is said to have been found. An example of a transverse mass plot is shown in Figure 4.2.

## 4.3 Structure of the proton

Proton is not a point-like elementary particle such as the electron but instead it has an internal structure, as was discovered at the Stanford Linear Accelerator Center with deep inelastic scattering experiments in 1968 [54]. Protons consist of two up-quarks and a down-quark called the *valence quarks*, kept together by the strong interaction i.e. the constant exchange of gluons. On top of that, these gluons can split into quark-antiquark pairs known as the *sea quarks*. When calculating the outcome of a proton-proton collision,

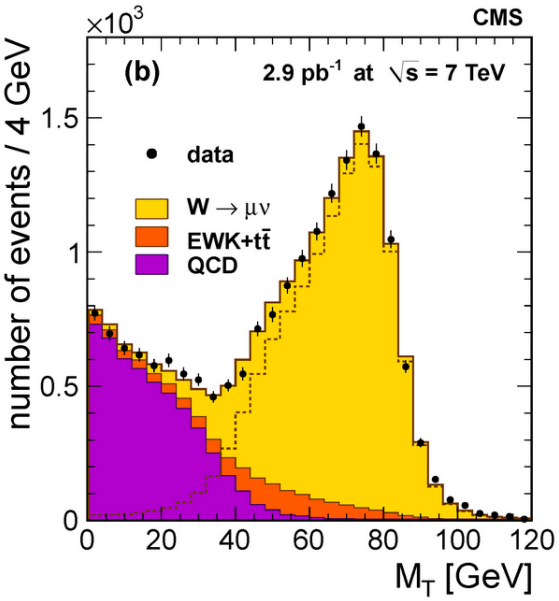


Figure 4.2: Example $m_T$ plot of the W boson signal at the CMS detector. The signal is in yellow while the electroweak and QCD backgrounds are shown in orange and purple respectively. [53]

one has to deal with a whole bunch of elementary particles, some of which interact in the collision. Difficulties arise as the proton momentum is distributed to all the constituent particles in some way and it is impossible to say which quarks or gluons participated in the interaction and what were their initial momenta.

The description of hadron collisions is possible using so called *factorization theorems* [55], that allow the separation of the long- and short-distance behavior from each other. This means that the short-distance interaction called the *hard interaction*, can be solved with the usual perturbative methods of asymptotically free QCD while the non-perturbative long-distance interactions are determined by datafits to experimental data.

The effect of long-distance interaction is encased into something referred to as the *parton distribution function* (PDF), named after the parton model first introduced by Richard Feynman in 1969 [56]. It gives the likelihood that a quark or a lepton carries a certain fraction of the total momentum of the hadron. After the PDF is determined at some energy scale from experimental data, the evolution of the PDF when the energy scale is changed is governed by Dokshitzer-Gribov-Lipatov-Altarelli-Parisi (DGLAP) equations [57–59].

Due to the colour confinement of the QCD, the data with proton-proton collisions will involve a lot of particles as the initially colour neutral protons are ripped apart in the collision. A cascade of new quarks has to be created from the energy involved in the quark field in order to restore the colour neutrality to all the particles coming out of the

interaction. This is called the *hadronization*. The cascades of particles are called *jets* as they are collimated and travel in the direction of the original particle causing the cascade, resulting in jet-like structures in the collision data.

# Chapter 5

# The Large Hadron Collider and the CMS detector

Located near Geneva on the Franco-Swiss border, The Large Hadron Collider (LHC) is the most powerful particle accelerator ever built. It is one of the accelerators operated at the European Organization for Nuclear Research (CERN) and houses various experiments dedicated to studying the laws of sub-atomic particle interactions and the structure of matter. The LHC is designed to collide protons into each other at 14 TeV collision energies.

The concept for the LHC was officially recognised in 1984 in a workshop held in Lausanne, Switzerland. In the workshop proceedings [60] the motivation for building a hadron collider capable of reaching collision energies of the 10 TeV magnitude were clear: To shed light upon the symmetry breaking mechanisms that are responsible for the masses of particles in the electroweak standard model, such as the Higgs mechanism.

The technology for building an circular accelerator capable of such energies required did not exist at the time. Especially the magnets required for accelerating and keeping the particles in a circular path would require much larger magnetic fields than yet available. Much work was needed before the energies for studying the symmetry breaking could be achieved in an accelerator.

More than ten years later, the LHC conceptual design was published [61] and many of the technical details had been decided. This new collider would be built into the tunnel formerly housing CERN's Large Electron-Positron Collider (LEP) and it would be capable of colliding protons at 14 TeV Center-of-Mass energy and lead ions at Center-of-Mass energies exceeding 1000 TeV. The LHC started operating for the first time in September 2008.

## 5.1 Structure of the accelerator

The accelerator consists of two acceleration rings going in opposite directions in the accelerator tunnel. Inside each ring there is a beam of protons separated into bunches of $10^{11}$ protons per bunch. These bunches are accelerated using radio frequency cavities and kept on a circular track by 1232 superconducting dipole magnets with 8.3 Tesla magnetic field strength. As the proton beams reach the desired energies, the beams are made to collide.

The two acceleration rings intersect at eight points. At these four of these interaction points, the proton bunches collide and variety of particle detectors observe the debris from the proton-proton interactions. The four main experiments at the LHC are situated at these interaction points: CMS, ATLAS, LHCb and ALICE. CMS and ATLAS are both general-purpose detectors studying a variety of different subjects. LHCb examines the difference between the amount of matter and antimatter in the universe, known as the baryon asymmetry. ALICE is specialized in studying heavy-ion collisions, where highly dense matter known as quark-gluon plasma is created at the asymptotically free region of QCD.

The LHC ring is only the final step in the acceleration chain for creating the energetic proton beams. At the point when the proton beams enter the LHC, they already have a kinetic energy of 450 GeV. There are in total four separate particle accelerators the particles go through before entering the LHC. The acceleration chain and the energy of the protons as leave each accelerator before the LHC ring is: Linac 2 (50 MeV), Proton Synchrotron Booster (1.4 GeV), Proton Synchrotron (25 GeV) and the Super Proton Synchrotron (450 GeV). The motivation for having so many accelerators for protons of different energies comes from optimizing the radio frequency cavities used in pushing the protons to higher and higher energies. The protons have to be in the range of 450 GeV when entering the LHC ring in order to be accelerated by its RF-cavities.

There are other experiments connected to the same accelerator complex than the ones described above. A diagrammatic picture of the complex is shown in Figure 5.1. These other experiments use the lower energy beams from the preaccelerators to the LHC to conduct various high energy physics and radiation experiments.

## 5.2 The CMS detector

The letter of intent for this general-purpose detector was presented by the CMS Collaboration in 1992 [63], and it was approved for one of the main detectors for the LHC. The main motivation for the CMS detector is to study the nature of electroweak symmetry breaking i.e. the Higgs mechanism and look for anything inconsistent with the Standard Model of particle physics, a clear signal of Beyond the Standard Model (BSM) physics.

The detector was designed with the demanding conditions of the LHC collisions in mind. Some of the aspects considered in making the detector were efficient $\tau$-triggering and tagging required for many search channels of the Higgs bosons, and of course good muon momentum resolution and identification as implied by the name of the detector. The main components of the detector and their purposes are presented concisely, as described in the CMS design report [64].

The subdetectors of the CMS can be presented as layers in the order that a particle emerging from the proton-proton collision in the interaction point would see them. This

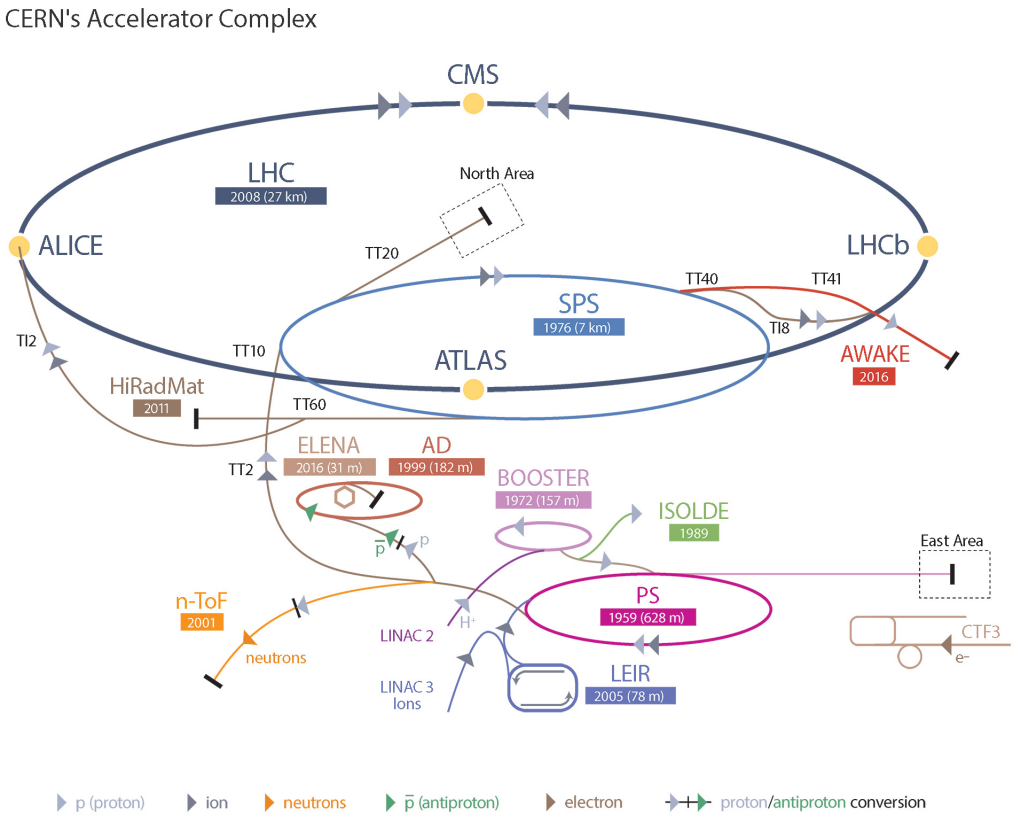


Figure 5.1: A diagram of the many experiments and accelerators at the CERN accelerator complex near Geneva. [62]

is an enlightening way to view the detector since different types of particles are stopped at different layers of the detector, dispatching their energies into the detector elements. This is demonstrated in Figure 5.2.

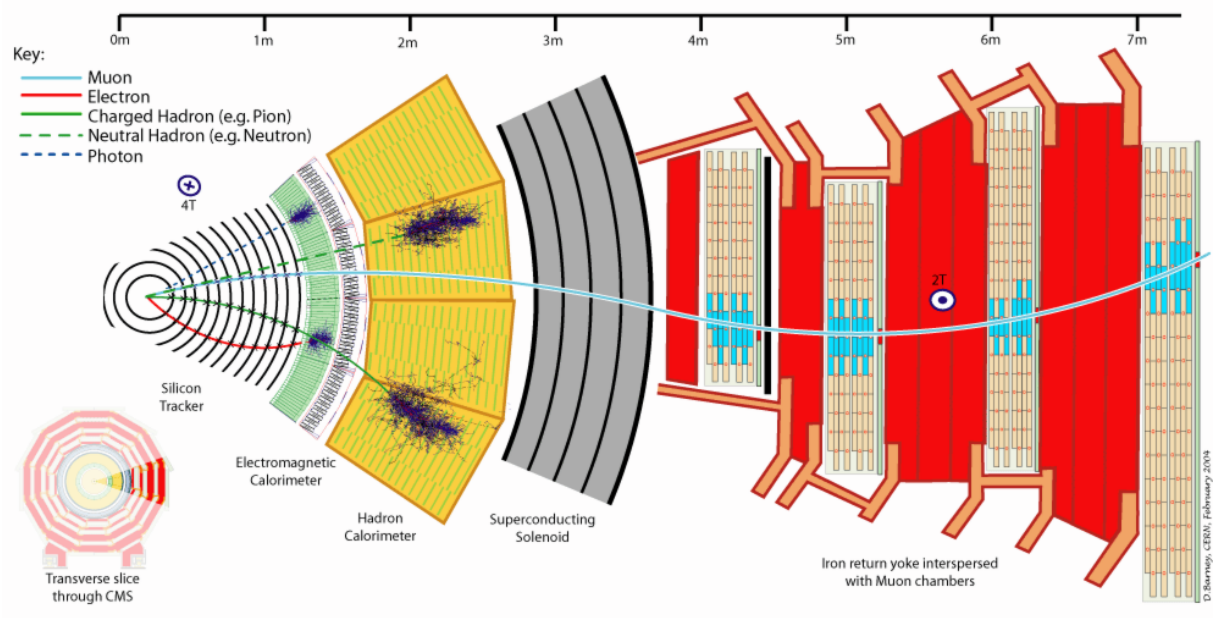


Figure 5.2: Cross cut slice of the CMS detector, showing how different types of particles propagate in the detector [65]

**Tracking system** surrounds the interaction point, extending to a radius of 1.1 meters from the beam pipe in the center of the detector. It is a silicon based tracker that operates by detecting small ionization currents caused by passing charged particles. With high granularity of the silicon components, measuring the currents from the individual silicon components allows the tracks of the charged particles to be determined up to very high accuracy. These components are called pixels or strips depending on their form. The innermost part of the tracker consists of silicon pixels while the outer region is made of silicon strips. The tracker has a spatial resolution of 10-30 $\mu$m for isolated muons of $p_{\mathrm{T}} = 100$ GeV/c and resolution of 10-12 $\mu$m in reconstructing primary vertices of interesting collision events [66].

With the tracks of the charged particles, *primary vertices* can be determined. They are the locations of proton-proton collisions in the beam pipe as well as *secondary vertices*, the locations where unstable, short-lived particles resulting from the primary vertices have decayed in the inner tracker. The tracker enables the calculation of charged particle momenta. Inside the CMS detector, the intense magnetic field curves the tracks of the particles due to the Lorentz force. After identifying the particle, its rest mass allows the momentum to be determined from the radius of curvature in the track.

There are in total ten layers of tracker material in the barrel region of the detector, four

in the inner tracker and six in the outer tracker. In the end-cap region there are 12 disk layers of pixel trackers, three inner disks and nine outer disks. The hit finding efficiency of the silicon layers were over 99% for the strip-layers and over 99.5% for the pixel-layers during the LHC Run-1 period [67].

**Electromagnetic calorimeter** (ECAL) is made of lead tungstate crystals ($PbWO_4$) scintillators that absorb energy from ionizing radiation, causing excited states in the crystals. These excited states re-emit the energy as blue-green light when returning to the ground state. This light is amplified by photodiode amplifiers and converted into a readout signal. The amount of light produced is proportional to the energy of the particle, allowing the energy of the particles to be determined from the readout signals. The ECAL stops the photons and electrons, while the more massive charged particles only deposit part of their energies to the crystals when passing through.

The crystals used in the ECAL are well suited for the extreme conditions of the LHC. The crystal material is highly dense (8.28 g/cm$^3$) and the electromagnetic showers caused by the absorbed energies are contained in small volumes i.e. the material has a small Molière radius. This allows for good granularity and a compact detector. The decay time for the excited states is of the same order of magnitude as the timing between bunches at the LHC, around 25 ns for most of the energy to be re-emitted. This fast response time is necessary to deal with the large particle flux. The material is also very radiation resistant so the ECAL should not suffer too large losses of sensitivity due to radiation damage.

The achieved energy resolution for electrons of $E_{\mathrm{T}} \approx 45$ GeV is less than 2% in the barrel region $|\eta| \leq 0.8$ and between 2-5% elsewhere. For photons of $E_{\mathrm{T}} \approx 60$ GeV the corresponding resolutions are 1.1-2.6% and 2.2-5.0 % [68]

**Hadron calorimeter** (HCAL) is built from alternating layers of absorber material and scintillator material. The hadrons hit the dense absorber material made of steel and brass, causing a shower of particles, which we can measure with the scintillator in the same way the ECAL measured electron and photon energies. There are in total 16 layers of scintillators in the HCAL. The calorimeter uses plastic scintillators instead of the lead tungstate crystals. These are not as radiation resistant as the $PbWO_4$ crystals, but as the ECAL already protects the HCAL from some of the radiation damage, this is not a problem. As materials with very high atomic numbers would cause muon momentum resolution to deteriorate in the multiple scattering region, brass was chosen as the absorber.

In addition to the usual barrel and endcap, the HCAL has forward region calorimeters extending the pseudorapidity region of the detector from $|\eta| = 3.0$ up to $|\eta| = 5.2$. In a proton-proton collision, on average 100 GeV is deposited to the barrel and endcap, where as the forward region calorimeter receives 760 GeV. This intense particle flux requires the forward calorimeter to be radiation durable. The calorimeter operates on detecting the

electromagnetic components of the particle shower by observing the emitted Cherenkov radiation.

The HCAL is much coarser than the ECAL resulting in poorer energy resolution. However the two subdetectors' data is combined when determining the energy for hadrons, resulting in energy resolution of the order 10% at $E_{\mathrm{T}} \approx 100$ GeV [69].

**Muon detector system** is the outermost component for CMS detector. Muons are able to penetrate most layers of the detector with little loss of energy, where as a large part of the other particles is stopped in the inner layers. Since the particles seen in the muon detectors are almost solely muons, they are relatively easy to detect. This allows high precision in interesting signal decays such as $H \to ZZ \to \mu^+\mu^+\mu^-\mu^-$.

The CMS utilizes three kinds of subdetectors for muons: cathode strip chambers (CSC), resistive plate chambers (RPC) and drift tubes (DT). All of these are gaseous particle detectors, operating by detecting ionization in the gas caused by a passing charged particle. The muon detector covers the pseudorapidity region of $|\eta| < 2.4$. The information from the inner tracker system is combined to the data from the muon detectors when reconstructing the muon momenta, in order to achieve high accuracy.

Total efficiency for muon reconstruction in pp collisions by the CMS detector is over 95% for muons with transverse momentum over few GeV/c. The energy resolution is between 1-6% depending on the pseudorapidity $|\eta|$ for muons $p_{\mathrm{T}} \leq 100$ GeV/c and under 10% for muons with transverse momenta $p_{\mathrm{T}} \leq 1$ TeV/c [70].

# Chapter 6

# Reconstructing collision data

In order to derive the physical content of the particle collisions from the data of the CMS subdetectors, so called Particle Flow (PF) technique is utilized. The detector information is used to construct all the stable particles of the event in a hierarchical way, and from these PF-candidates the higher level physics objects that have decayed in the detector can be constructed for further physics analysis'. The Particle Flow technique is a flexible approach to the analysis since the PF-candidate information can be used to later analyse the jet structure or change the parameters of reconstruction algorithms for unstable particles.

A good $\tau$-reconstruction efficiency is deemed very important in the CMS detector, as many of the particles beyond the Standard Model could show up as an excess of taus compared to the Standard Model prediction. This is also the case with the charged Higgs boson. The particle reconstruction in the CMS detector is described in the following section, focusing on the aspects important to $\tau$-reconstruction.

A schematic picture of how the reconstruction of the collision data through the PF-algorithms and the analysis of these objects leads back to the collision that took place inside the detector is presented in Figure 6.1.

## 6.1 Particle-Flow event reconstruction

The need for accurate PF-candidate reconstruction is obvious since all further analysis is based on these objects. The main aspects of the PF-algorithm [72], are reviewed here.

An important subdetector in determining the momenta of particles and the primary interaction vertices is the pixel tracker. The charged hadrons hit the tracker before the magnetic field has time to curve their paths, allowing simple measurements of flight directions of the particles from a vertex. The pixel tracker has also a good resolution required for accurate track determination.

The charged particles deposit energy to the pixel tracker when they pass through. These depositions are called *hits* and by combining hits on different layers of the tracker the path of the particle can be determined. The CMS PF-candidate reconstruction utilizes the iterative tracking strategy [66], where the original tracks are chosen with strict criteria from the detector hits so that the fake rate is kept small. The signals matching these tracks are then removed from the data and the next round of matching the detector hits into a

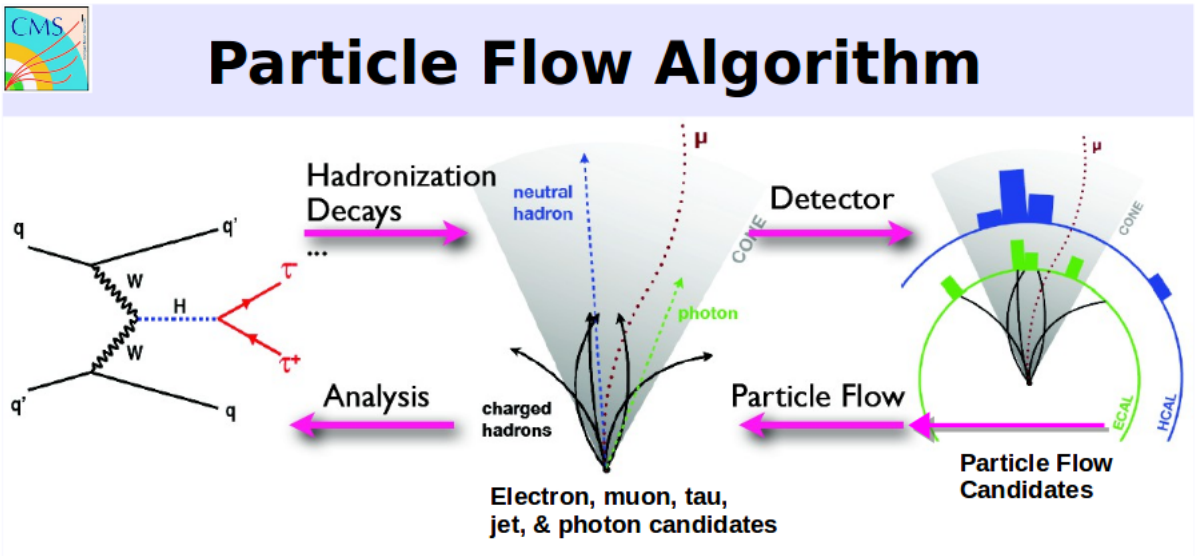


Figure 6.1: Demonstration of how the physical interaction of the colliding protons shows up in the detector and is reconstructed through the PF-algorithm to allow the analysis of the event [71].

continuous particle track is performed with slightly more loose criteria. Repeating this process results in a good track reconstruction efficiency with a relatively low fake rate. Especially for isolated muons this leads to an impressive $\sim$ 99% efficiency [73]. As the magnetic field causes the paths of the charged particles to curve, their momenta can be calculated from the curvature radius when the track is extended to take into account the hits in the outer detector elements.

The tracker information is combined to the data from the other subdetectors, checking that the tracker hits correspond to energy deposits in these instruments. By starting from the particles with the clearest signals and removing the detector data used after reconstructing the PF-candidate from consideration, this process can be done efficiently even for the large amounts of data received from the CMS detector.

**Muons** can be identified using the muon chambers and the tracker data. An event where a charged particle that is not a muon causes a signal in the muon chambers is called a *punch-through event* but it is a relatively unlikely occurrence. This leads to a signature, where muons leave hits on the inner tracker layers and the muon systems, but only small energy deposits in the calorimeters in between. If a muon chamber track can be linked to a signature in the tracker, a *global muon* candidate is constructed. Such global muon candidates are reconstructed as PF-muons if they satisfy the conditions of the *Tight Muon selection* [74] which require for example certain amount of hits in the trackers and $|\eta|$ to be within the sensitive region of the detector.

**Electrons** are the lightest charged particles in the detector and as such they emit Bremsstrahlung when interacting with the magnetic field. These photons deplete the electron energy in between tracker elements so the trajectory curvature radius is seen to diminish. The photons are emitted tangentially with respect to the electron trajectory curve and they leave energy deposits spread in the $\phi$ direction to the ECAL subdetector. A Gaussian-Sum-Filter (GFS) [75] is used to refit the electron candidate trajectory and if the ECAL and tracker data agree, a PF-candidate electron is constructed. Due to the transition region between the barrel and the end-cap of the ECAL detector, electron candidates within pseudorapidity $1.4442 < |\eta| < 1.5660$ are removed.

**Photons** are neutral particles and such they do not cause hits in the tracker elements. They are however absorbed by the ECAL subdetector, so energy deposits there that are not matched with other particle tracks will be considered as photons. However when the photons are energetic enough, they can convert into a $e^+e^-$ pair. This is known as the *photon conversion* and up to $\sim 70\%$ of the photons mediating the tracker undergo this process [76]. This effect is taken into account in the photon reconstruction algorithms using the ECAL and tracker data [77].

**Charged hadrons** can be identified from the tracker and HCAL signals that remain after the aforementioned particles have been reconstructed into PF-candidates. Even though charged, the hadrons deposit little energy to the ECAL detector elements.

**Neutral hadrons** give a signal where there are no hits in the tracker but energy deposits in the HCAL elements. After the tracks and calorimeter signals of the above mentioned particles that are somewhat easier to detect directly, the excess energy in the calorimeter can be assigned into neutral particles and removed from consideration.

**Primary vertices** are constructed with a *deterministic annealing* method [78], where artificial neural networks are utilized in clustering tracks together. The vertex with the largest sum of the squares of the transverse momenta is chosen as the signal primary vertex. The reconstructed vertices must fulfil the conditions

- The transverse distance from the beam pipe $|\rho| < 2$ cm.
- The longitudinal distance from the nominal interaction point $|z| < 24$ cm.
- The degrees of freedom $n_{\text{dof}} > 4$ for the vertex, where

$$n_{\text{dof}} = -3 + 2 \sum_{i}^{\#tracks} w_i$$

.

The $w_i$ are weights given to the tracks, with the tracks closest to the vertex getting the highest weights. As the physical content of the interactions is derived from the outgoing particles from the vertex, a good performance in clustering the correct tracks to the same vertex is vital for the analysis.

**Jets** in the event are reconstructed by clustering the PF-candidates in the event with a anti-$k_{\mathrm{T}}$ algorithm [79] with jet size parameter $R = 0.4$. Algorithm combines PF-candidates into jets satisfying the identification conditions [80], where the energy distribution and particle content in the jet is examined and required to fit within certain parameters. The combined particles are determined by calculating distance parameters between nearby particles and linking them into a jet should the distance parameter be small enough. Due to detector effects, the reconstructed jet energies do not completely match the true jet energy and jet energy scale corrections are performed when analysing data [81].

Due to the structure of the proton and the colour confinement of the QCD presented before, jets are very common in hadron collision data. Understanding and reconstructing jets in the detector is then crucial for analysing the results.

**B tagging** is required for identifying events with b-quarks resulting in jets. In the $\mathrm{t\bar{t}}$ events, there ar two jets originating from the b-quarks that the t-quarks decay into. The b jets are found and identified using the *Combined Secondary Vertex* algorithm [82]. It reconstructs the secondary vertex where the b-quark decays using the charged tracks and their impact parameters. Due to the finite lifetime of the b-quark the tracks from the secondary vertex are clustered away from the primary vertex. As b-jets are present in many events of interest, they are identified in this early stage of the analysis in order to separate possibly interesting collision events from the rest.

**The missing transverse energy** can be determined after the reconstruction of all the particles described above. Since the initial total momentum of the collision is very close to zero in the detector's frame of reference, the negative vector sum of the constructed particles' momenta is defined as the missing transverse energy $E_{\mathrm{T}}^{\mathrm{miss}}$. The $E_{\mathrm{T}}^{\mathrm{miss}}$ of an event contains the contributions from neutrinos that do not interact with the detector, known causes for mismeasurements resulting in missing energy and other sources such as cosmic rays passing through the detector [83]. A good performance in measuring the missing energies is a priority as many searches for new physics assume a signature of large missing energy in the event.

## 6.2 $\tau$-jet reconstruction

The higher level physics objects are constructed from the PF-candidates. As the $\tau$ lepton has a relatively short lifetime, its mean lifetime at rest being $2.91 \times 10^{-13}$s [84], the signal tau leptons with high energies usually propagate distances of a few millimeters before decaying. This is not enough to reach the detector elements. The final states are hadronic; neutral and charged pions with a tau neutrino, in about two thirds of the time.

A specialized hadrons-plus-strip (HPS) algorithm [85] is used in reconstructing the $\tau$ jets from the PF-candidates, taking special care in identifying the photon conversion in the

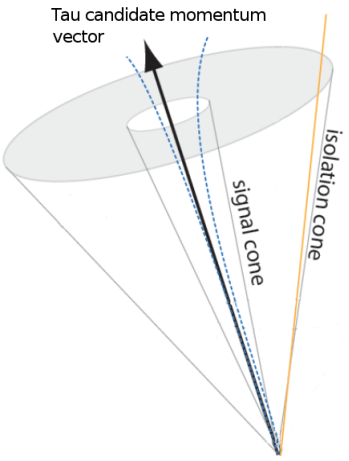


Figure 6.2: The signal cone and the isolation cone around the tau candidate. Figure modified from [86]

detector. In this process combinations of the reconstructed PF-candidates are matched with possible $\tau$ decay channels. If the PF-candidates match a possible tau decay, $\tau$-candidate is formed with the 4-momentum calculated as the sum of 4-momenta of the PF-candidates used for the reconstruction. For the constructed $\tau$-candidates, discriminators separating $\tau$-decays from signals caused by electrons, muons and gluon or quark jets are used.

The PF-candidates used in the reconstruction of a $\tau$-candidate are required to be within $\Delta R \leq 3.0/p_{\mathrm{T}}[\mathrm{GeV}]$ around the $\tau$ -candidate momentum vector with lower and upper limits of $0.05 \leq \Delta R \leq 0.10$. This is to account for the effect of higher energy tau particles decaying into more collimated jets. The cone defined by $\Delta R$ is called the *signal cone*. Tau decays in the detector can be mostly separated from QCD-jets by defining an *isolation cone* around the tau candidates. A cone of $\Delta R \leq 0.5$ is formed around the tau candidate momentum vector and the sum transverse momentum of charged particles and photons exceeding $p_{\mathrm{T}} \geq 0.5$ GeV that are outside the signal cone and inside the isolation annulus is calculated. Then the strictness of the isolation condition is defined as loose, medium or tight working points, requiring the sum of the momenta to not exceed 2.0, 1.0 or 0.8 GeV respectively. This isolation cone discriminates between taus, that form very narrow collimated jets, from the QCD jets that tend to be more spread out after the hadronization. The signal cone and isolation annulus around the tau candidate are visualised in Figure 6.2.

The used tau reconstruction and identification methods in CMS achieve identification efficiency of 50-60% for tau leptons and misidentification rates between per mille and per cent level for quark and gluon jets, muons and electrons. [85]

# Chapter 7

# Searching for the Charged Higgs boson in the $H^{\pm} \to \tau^{\pm}\nu$ fully hadronic -channel

The search channel described here assumes the decay of charged Higgs bosons into tau and neutrino $H^+ \to \tau\nu_\tau$, and the subsequent decay of the tau lepton into hadrons $\pi^+$ and $\pi^0$. The mass of the charged Higgs bosons can be reconstructed in the transverse plane and possible finding of the charged Higgs boson would result from a large enough deviation from the transverse mass distribution of taus and neutrinos predicted by the Standard Model. The notation $H^+$ is used to refer both negatively and positively charged Higgs boson.

The mass of the charged Higgs boson is one of the parameters left free by the supersymmetric extensions. Experimentally the lower limits have been determined by excluding $m_{H^+} < 78.6$ GeV [87–90] in a model independent way, while the upper limit of the mass is set on theoretical grounds to around ∼1 TeV in order to restrict the amount of fine-tuning in the theories. The analysis for charged Higgs boson seaches presented here is restricted into the mass window 80 GeV $\leq m_{H^+} \leq$ 500 GeV.

The mass of the charged Higgs boson determines its dominant production mechanism and decay channels. Two different cases divided as *light charged Higgs boson* and *heavy charged Higgs boson* are studied. Depending on the mass of the charged Higgs boson, there are various backgrounds that will obstruct the detection of the signal. The main backgrounds and the event selection methods designed to separate the signal from the backgrounds are presented. The studied collision events have the center of mass energy of 13 TeV and the data from 2015 is used in the fake tau background measurements.

## 7.1 Signal

Depending on the mass of the charged Higgs boson, the production and decay channels differ. The defining factor is whether the Higgs mass is less than the mass difference of top and bottom quark masses $m_{\mathrm{H}^+} \leq m_{\mathrm{t}} - m_{\mathrm{b}}$ so that top quarks can decay as $\mathrm{t} \to \mathrm{H}^+\mathrm{b}$. In this mass region the charged Higgs boson decays preferentially to tau lepton and a tau neutrino, causing an excess of taus in $\mathrm{t\bar{t}}$ events in comparison with the Standard Model prediction.

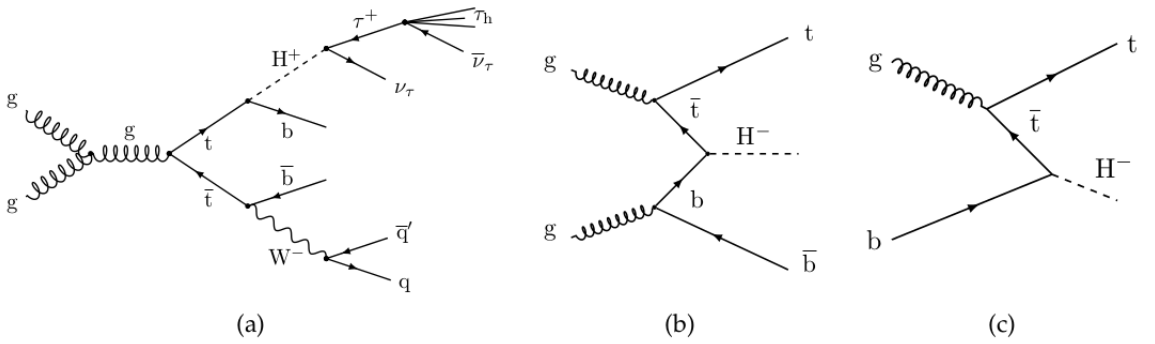


Figure 7.1: a) Light charged Higgs boson production through $t \to H^+b$. b) Heavy charged Higgs boson production in 4 flavour scheme through $\bar{t}b \to H^+$. c) Heavy charged Higgs boson production in 5 flavour scheme through $\bar{t}b \to H^+$. [92]

If the charged Higgs boson mass is larger than the difference of top and bottom quark masses, $m_{H^+} > m_t - m_b$, the main production mechanism for charged Higgs bosons is through bottom and anti-top (or top and anti-bottom) quark fusion. In perturbative QCD processes involving bottom quarks, the calculations are done in different flavour schemes that give identical predictions when calculated to all orders of perturbation theory, but differ in finite orders. In the CMS analysis for the charged Higgs boson, the four flavour scheme (4FS) and five flavour scheme (5FS) are combined with Santander matching method [91]. In the 4 flavour scheme the b-quark production is calculated perturbatively from a quark splitting into $b\bar{b}$ pair, while in the 5 flavour scheme approach the b-quarks are treated as partons with the four lightest quarks so the quark-sea includes a certain number of b-quarks that can participate in the charged Higgs boson production.

The different production mechanisms for the charged Higgs boson production are presented in Figure 7.1 for the light charged Higgs boson and heavy charged Higgs boson in 4 four flavour scheme and in 5 flavour scheme.

In all of the scenarios the presence of the charged Higgs boson would cause an excess of tau leptons in the data. As the taus decay dominantly into hadronic channels, observing the hadronic tau jets give a good discovery potential. The hadronically decaying tau is denoted as $\tau_h$. A problem in this decay channel is that it overlaps with the large background from QCD-jet events, but as the tau jets tend to be more collimated, the isolation requirements used in tau jet reconstruction give reasonable discriminating power against the QCD background.

The charged Higgs boson decays into a tau and a neutrino, which is detected through the missing transverse energy of the event. If there are no other sources $E_{\mathrm{T}}^{\mathrm{miss}}$, the transverse mass for the charged Higgs boson can be reconstructed from the signal tau $p_{\mathrm{T}}$ and the $E_{\mathrm{T}}^{\mathrm{miss}}$ in the event.

## 7.2 Backgrounds

Dominant backgrounds in searching the signal from hadronic tau decays are given by QCD multijets and electroweak (EWK) processes causing jets. The EWK processes are W + jets, single top, Z*/$\gamma$ and diboson WW, WZ and ZZ events. The background can be divided as fake tau and genuine tau backgrounds, depending on whether the tau lepton in the event is due to misidentification or a real tau production process. These backgrounds with the signal from a charged Higgs boson is presented in Figure 7.2.

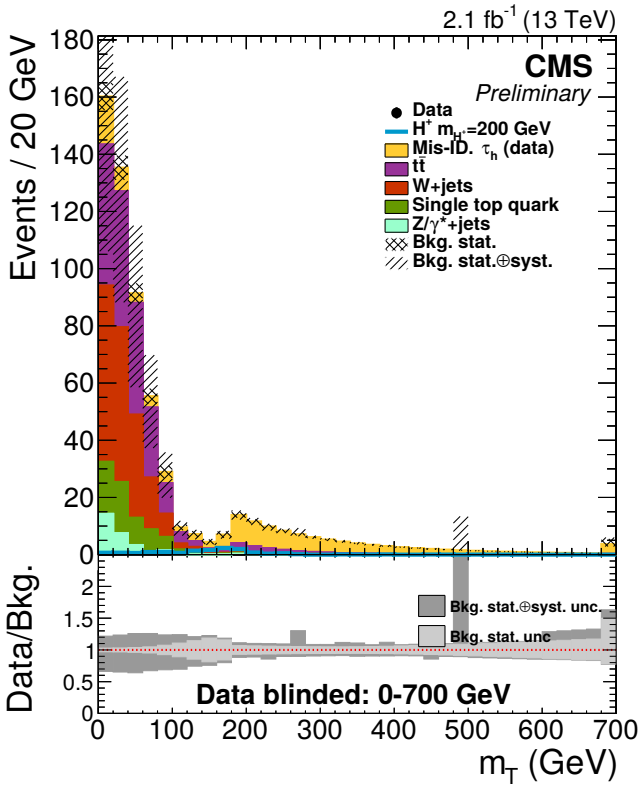


Figure 7.2: Backgrounds when searching charged Higgs boson in the hadronic tau decays at 13 TeV center of mass energy. The fake taus are contained in the data-driven Mis-ID. $\tau_h$ background and the true tau events in the rest of the backgrounds that are simulated. The charged heavy Higgs boson with $m_{H^+} = 200$ GeV/c$^2$ is used as the signal.

**QCD multijet** background is an inevitable nuisance in hadron collisions due to colour confinement and the hadronization of the quarks. As mentioned the QCD background is suppressed in check through the isolation condition when constructing tau jets.

**EWK+t$\bar{\text{t}}$ with genuine tau** background is called the *irreducible background* when analysing the tau channel for the signal. Since taus are the signal particles that are being searched for the reconstruction of the charged Higgs boson mass, it is especially

hard to discriminate the signal taus against this background. It is in order to reduce this background that the tau veto method studied for this thesis is intended.

**EWK+$\mathbf{t\bar{t}}$ with fake tau** background is caused due to the misidentification of some other particle or jet as a tau. The better the tau reconstruction algorithms, the lesser the effect of this background in the analysis will be.

The background measurements are to be done using data-driven techniques. The QCD multijets with fake tau and the EWK+$t\bar{t}$ with fake tau can be determined using *inverted selection*, where the events satisfying all the selection conditions except tau isolation are chosen. This leads to a sample of events dominated by the fake tau events. The EWK+$t\bar{t}$ with genuine tau background is measured using observed muon events where the muon is replaced using *tau embedding* insert a tau particle into the event. [93]

## 7.3 Event selection

For a collision event to be considered interesting enough to be used in the analysis of the charged Higgs boson, it has to pass the trigger designed to look for such events. Events passing the trigger must have:

- Loosely isolated PF-candidate tau with $p_{\mathrm{T}} > 50$ GeV/c.
- Number of charged prongs in the tau candidate is less than four.
- Leading charged track $p_{\mathrm{T}} > 30$ GeV/c and $|\eta| < 2.1$ in the signal tau.
- Missing transverse energy $E_{\mathrm{T}}^{\mathrm{miss}} > 80$ GeV.

The conditions for selecting events for the analysis from those passing the trigger are chosen so that the background events and events with large mismeasurements of $E_{\mathrm{T}}^{\mathrm{miss}}$ are separated from the signal events of good quality:

- Loosely isolated $\tau_{\mathrm{h}}$ with $p_{\mathrm{T}} > 60$ GeV/c, $|\eta| < 2.1$ is present in the event.
- The $\tau_{\mathrm{h}}$ is associated to one charged hadron and it has $p_{\mathrm{T}} > 30$ GeV/c.
- Particle Flow $E_{\mathrm{T}}^{\mathrm{miss}} > 120$ GeV in the event.
- No isolated electrons (muons) with $p_{\mathrm{T}} > 15$ (10) GeV/c.
- At least three jets with $p_{\mathrm{T}} > 30$ within $|\eta| < 2.1$ in addition to the $\tau_{\mathrm{h}}$ jet. One or more of them is b-tagged.
- $\vec{E}_{\mathrm{T}}^{\mathrm{miss}}$ and jet directions satisfy the angular cuts $R_{\mathrm{bb}}^{\mathrm{min}} > 40°$, $R_{\mathrm{coll}}^{\mathrm{min}} > 40°$,

where

$$R_{\mathrm{bb}}^{\mathrm{min}} = \sqrt{\left(\pi - \Delta\phi(\tau \text{ jet}, \ \vec{E}_{\mathrm{T}}^{\mathrm{miss}})\right)^2 + \left(\Delta\phi(\mathrm{jet}_n, \ \vec{E}_{\mathrm{T}}^{\mathrm{miss}})\right)^2},$$

$$R_{\mathrm{coll}}^{\mathrm{min}} = \sqrt{\left(\Delta\phi(\tau \text{ jet}, \ \vec{E}_{\mathrm{T}}^{\mathrm{miss}})\right)^2 + \left(\pi - \Delta\phi(\mathrm{jet}_n, \ \vec{E}_{\mathrm{T}}^{\mathrm{miss}})\right)^2}$$

and $\mathrm{jet}_n$, $n = 1, 2, 3$ refers to the three highest $p_{\mathrm{T}}$-jets in the event.

Large missing transverse mass in the $\tau\nu$-channel is a signature of the charged Higgs boson due to the neutrinos from its decay. The requirement of at least three jets in total with at least one tagged as a b jet allows the selection of the $\mathrm{t\bar{t}}$-like events, where the excess of taus due to charged Higgs boson is expected to be observable. The angular cuts suppress the events where $\vec{E}_{\mathrm{T}}^{\mathrm{miss}}$ is reconstructed due to mismeasurement, when it tends to be in the direction of the tau or one of the other jets.

The events with isolated electrons and muons are removed as they are always accompanied by their corresponding neutrinos, which would affect the transverse mass reconstruction of the charged Higgs boson through $E_{\mathrm{T}}^{\mathrm{miss}}$. This is also necessary in order to be able to combine the results from the study of fully hadronic decay modes of the charged Higgs boson to the studies performed in leptonic decay channels without overlap.

## 7.4 Tau veto

Since $E_{\mathrm{T}}^{\mathrm{miss}}$ is used in the reconstruction of the transverse mass distribution, all the inaccuracies in determining $E_{\mathrm{T}}^{\mathrm{miss}}$ affect the analysis when searching for the signal events. One aspect to be considered is the case for the events with more than one lepton. These events will also have a corresponding number of lepton neutrinos that contribute to the missing energy of the event. In the transverse mass reconstruction, the missing transverse energy is associated to the neutrino from the signal event, so multiple neutrinos can decrease the transverse mass resolution.

Events with more than one tau lepton are possible in the selected events for the charged Higgs boson analysis and if the tau neutrinos are emitted into roughly the same direction, the value for $E_{\mathrm{T}}^{\mathrm{miss}}$ grows. This effect can cause some of the background events to be reconstructed into higher transverse masses overlapping the transverse masses of the $\mathrm{H}^+$ signal. The goal of a tau veto is to reduce this kind of events.

As the neutrinos are not directly detected by the CMS, reducing the distortion in the $E_{\mathrm{T}}^{\mathrm{miss}}$ and its effect on quantities reconstructed using it has to be done indirectly. Since large missing transverse energy is expected from the Higgs signal, direct cuts by setting maximum value for $E_{\mathrm{T}}^{\mathrm{miss}}$ when selecting events will not improve the analysis. A possible

method would be to remove all events with more than one reconstructed $\tau$ particle from the analysis using a tau veto condition. Even though the signal tau used in the event selection was 1-pronged, both 1-pronged and 3-pronged taus can be present in the events studied.

To evaluate the usefulness of such a tau veto, the improvement of significance and the increase in systematic uncertainty of the whole analysis chain has to be considered. Vetoing the events with more than one tau will of course remove some of the signal too, which is taken into consideration when calculating the significance. The effect of tau veto is studied by using simulated data samples for the charged Higgs boson signals and $\mathrm{t\bar{t}}$ jets with genuine taus, in order to determine the change in significance from using this method. For the light charged Higgs boson scenario, masses $m_{\mathrm{H^+}}$=[80, 100, 120, 140, 160] GeV/$\mathrm{c}^2$ are considered and for the heavy charged Higgs boson the masses are $m_{\mathrm{H^+}}$=[180, 200, 220, 250, 300, 350, 400, 500] GeV/$\mathrm{c}^2$.

# Chapter 8

# Results

## 8.1 Statistical significance and systematic uncertainties

The $t\bar{t}$ background contains many events with more than one tau lepton, as both top-quarks can decay into taus via W-bosons. It is also the largest background that can include two taus after the event selection and it will be used as an example background when studying the effect of tau veto on the analysis. However the limit calculations presented in this section are done with all the backgrounds present.

The transverse mass distribution for reconstructed tau particles in $t\bar{t}$ event sample when all the events with more than one generator level tau were removed is shown in Figure 8.1. In the high transverse mass tail ($m_T \geq 100$ GeV/$c^2$), the number of events is reduced by 43% with this removal. This is to be considered the ideal case scenario giving the upper limit of possible background reduction in $t\bar{t}$ background events in the high $m_T$ tail using a tau veto. The removal of the events could result in a better signal-to-background ratio as the high $m_T$ tail overlaps the mass region of the $H^+$ signals.

For the light charged Higgs boson signal, the relevant background is around $m_T = 60-180$ GeV/$c^2$ instead of the high energy tail. In this region the reduction in background events is 26%.

The efficiency of tau reconstruction and identification is 50-60% at the CMS [85] so that in events with multiple taus the identification of more than one tau is not always successful. The distribution of the transverse momentum $p_T$ for the identified and unidentified taus for a sample of $t\bar{t}$ event taus after all the selections is shown in Figure 8.2. The identification efficiency as a function of transverse momentum is shown in Figure 8.3. It is seen that a majority of the unidentified taus have small transverse momenta ($p_T < 20$ GeV/$c^2$). As the tau reconstruction algorithm is not even seeded by tau jets with $p_T < 14$ GeV/c, the large number of unreconstructed taus in that region is not surprising. The trigger also affects the number of identified taus at low $p_T$ values. Even though the trigger and the event selection do not accept events without taus with transverse momenta $p_T \geq 50$ GeV/c and $p_T \geq 60$ GeV/c, there can be taus with lower momenta present in the events where the signal tau satisfies the momentum conditions.

When the transverse momentum is low, the decay products of tau particles are not necessarily collimated enough to allow efficient discrimination from the QCD background. The reason for this can be determined from the kinematics of decaying particles. Using as a simple example the decay $\tau \rightarrow \pi^+\pi^0\nu_\tau$, the angle $\theta_\pi$ between the direction of the

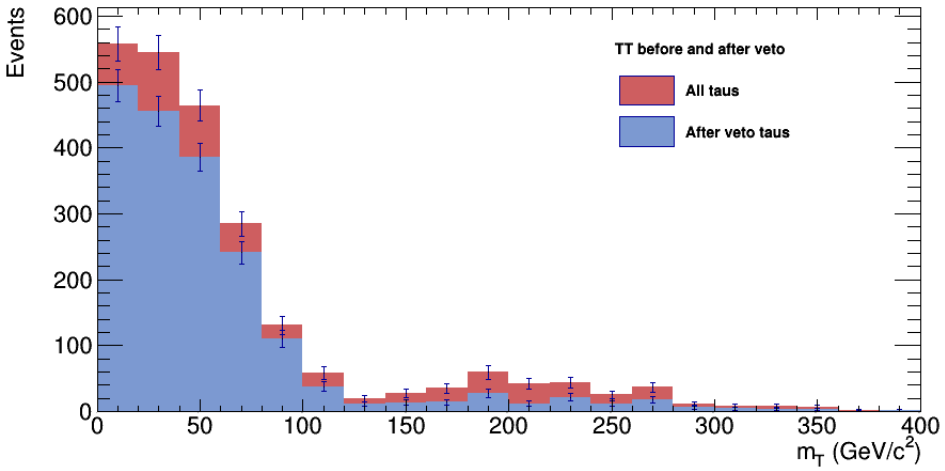


Figure 8.1: Comparison between the transverse mass of reconstructed taus from all $t\bar{t}$ events passing the selections and from $t\bar{t}$ events with only one tau. A decrease of 43% in event rate in the tail $m_T \geq 100$ GeV/$c^2$ and a decrease of 26% in event rate in the $m_T = 60 - 180$ GeV/$c^2$ region are observed in the reconstructed taus.

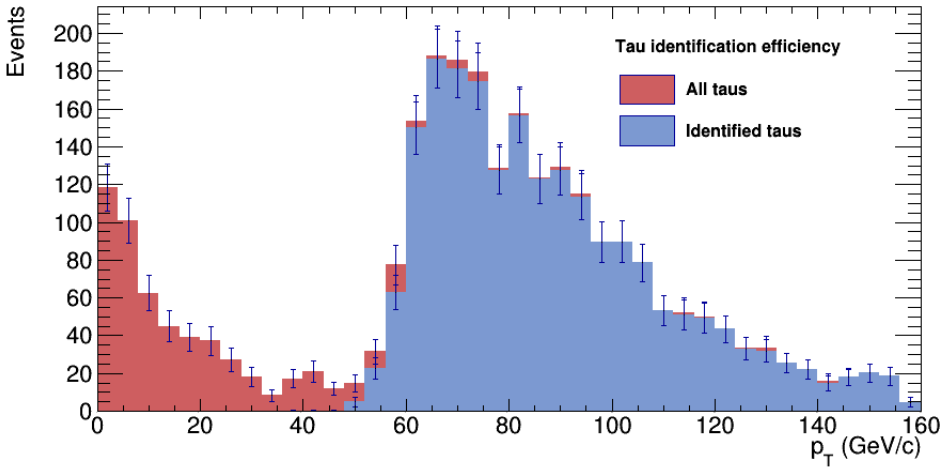


Figure 8.2: A large portion of the unidentified taus (shown in red) after the event selection have a relatively small transverse momentum $p_T \leq 60$ GeV/$c^2$. The distribution of identified taus shows the effect of the trigger selection at tau $p_T > 50$ GeV/c. The sub-leading tau is unaffected by the trigger, and shows the exponentially decreasing distribution as a function of tau $p_T$. A sample $t\bar{t}$ events was used for this distribution.

visible part of the tau and a decay product pion in the detector frame of reference has the relation

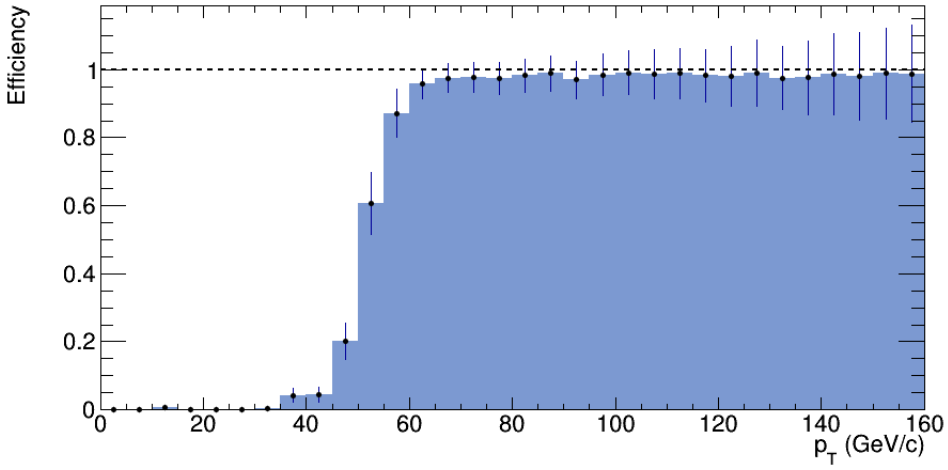


Figure 8.3: Identification efficiency of taus as a function of transverse momentum shown for a $t\bar{t}$ event sample. The rapid decrease of the efficiency below 60 GeV/c is caused by the trigger turn-on.

$$\theta_\pi \propto \arctan\left(\frac{1}{|\bar{p}_\tau|}\right), \tag{8.1}$$

due to Lorentz boost from the tau rest frame to the detector rest frame. So the smaller the momentum of the tau in the detector, the larger the decay angle is for the daughter particles. When the decay angle is large, the jet is not considered collimated enough to discern reliably from QCD jets to be reconstructed as a tau particle.

The low $p_\mathrm{T}$ and deviation of the decay products from the visible tau direction give some insight to why all taus are not identified, as the risk of misidentification becomes higher at lower $p_\mathrm{T}$ values. However since the possible advantages through removal of the events with more than one tau were shown to be significant, one should try to estimate how much could be achieved in a best case scenario, with the imposed limitations to the identification discussed above.

### 8.1.1 An optimistic tau veto using charged tracks

To estimate the effect of a tau veto using charged tracks, an assumption is made that all of the charged tracks within $\Delta R \leq 0.1$ of the visible tau direction could be used successfully to identify the excess taus in events with multiple taus. A $t\bar{t}$ event sample is used as a background in this estimation. A limit calculation for the expected cross section before and after the tau veto with all the backgrounds present is also presented at the end of this section. Using generator level information to match charged tracks with visible taus,

4.4% of the $t\bar{t}$ jets background events in the high energy $m_T \geq 100$ GeV/$c^2$ tail and 2.2% of the events in the region $m_T = 60 - 180$ GeV/$c^2$ can be vetoed. The effect of the tau veto on the reconstructed transverse masses is presented in Figure 8.4. As the veto is performed using generator level information of the existence of a tau in the event, this has no effect on the fake tau backgrounds.

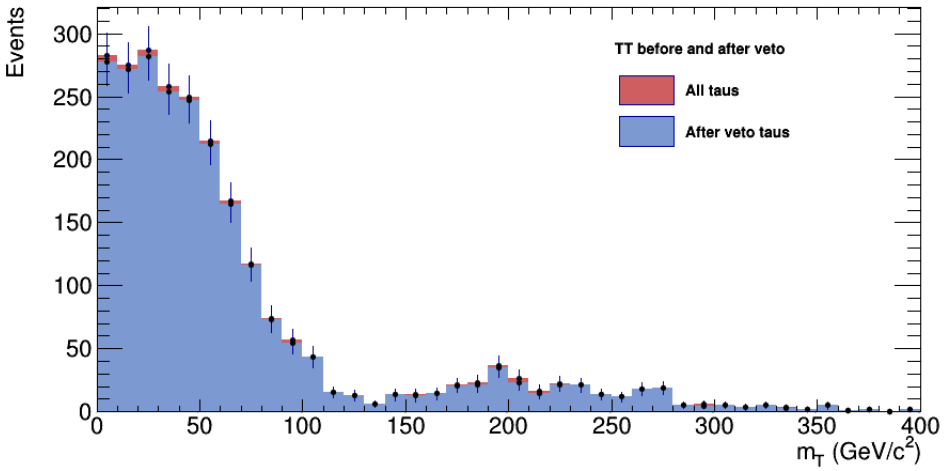


Figure 8.4: The effect of the optimistic tau veto on $t\bar{t}$ events. Only a small fraction of the missing taus are seen from charged pion tracks in generator level tau directions.

The low percentage of vetoed events compared to the number of events with more than one tau can partly be understood through the nuclear interactions of the charged pions with the detector. The CMS detector material corresponds to between $0.4X_0$ at $\eta = 0$ to $1.8X_0$ at $|\eta| \approx 1.5$ interaction lengths for the charged pions. This complicates the reconstruction of charged pion tracks in the detector especially in for the low transverse momenta $p_T \leq 0.9$ GeV/c pions [94] and many of the low $p_T$ taus cannot be identified even in this optimistic scenario.

An example distribution for the transverse mass calculated using reconstructed taus in this scenario are shown in Figure 8.5. A heavy charged Higgs boson of mass $m_{H^+} = 180$ GeV/$c^2$ was used as the signal. The transverse mass distributions after a tau veto for all the different light and heavy charged Higgs boson masses studied are collected into appendix A. The event rates were normalized to $\mathcal{B}(t \to H^+b) \times \mathcal{B}(H^+ \to \tau^+\nu_\tau) = 0.01$ for the light charged Higgs boson and $\sigma(pp \to \bar{t}(b)H^+) \times \mathcal{B}(H^+ \to \tau^+\nu_\tau) = 1$ pb for the heavy charged Higgs boson.

As the (anti)top quark decay can result in a tau lepton via intermediate $W^+$ ($W^-$) boson, the charged Higgs boson signal events can also contain more than one tau. The percentage of the $H^+$ events vetoed with the same conditions are presented in the Tables 8.1 and 8.2. In the light Higgs boson scenario, the highest $p_T$ tau used in transverse mass reconstruction is actually from the $W^\pm$ boson in around 4-11% of the events, depending on the charged Higgs boson mass. This causes the number of removed events in the mass window to vary

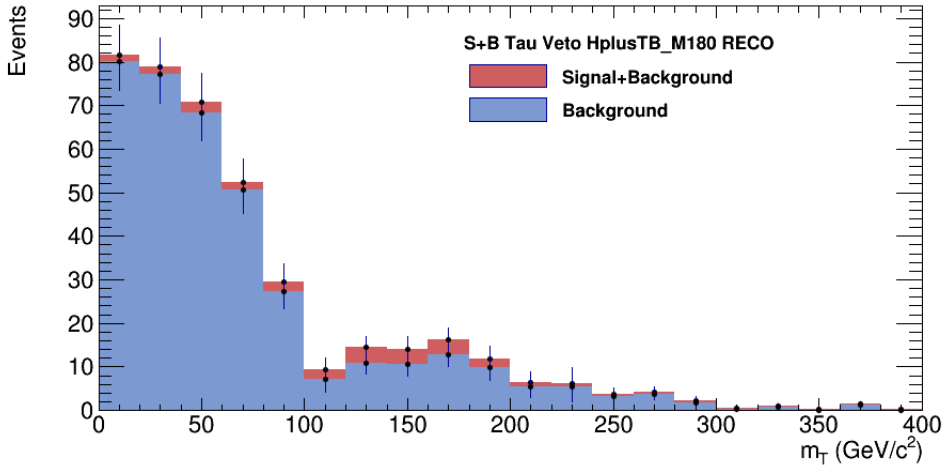


Figure 8.5: The transverse mass distribution for the signal+background and the background only, where the background contains only $t\bar{t}$ events after the event selection and tau veto. The heavy charged Higgs boson with a mass of $m_{H^+} = 180$ GeV/c$^2$ was used as the signal. Transverse mass reconstruction was done using reconstructed taus after a tau veto on events with more than one tau, under the assumption that all the charged tracks withing $\Delta R \leq 0.1$ from the visible generator tau direction could be identified as taus. This removes 4.4% of the events from the $m_T \geq 100$ GeV/c$^2$ and 2.2% of the events in the region $m_T = 60 - 180$ GeV/c$^2$ from the $t\bar{t}$ jets background.

| Light charged Higgs boson ($m_{H^+}$) | Removed (%) | $\Delta_{sig}$/sig (%) |
|---|---|---|
| 80 | 2.1 | -1.0 |
| 100 | 2.0 | -0.9 |
| 120 | 1.3 | -0.2 |
| 140 | 1.8 | -0.7 |
| 160 | 0.6 | 0.5 |

Table 8.1: The percentages of removed events from the signal and the increase in significance. For light charged Higgs boson, the mass window $m_{H^+} = 60 - 180$ GeV/c$^2$ was used, where the percent of removed $t\bar{t}$ jet background is 2.2%.

instead of being the same 2.2% found for $t\bar{t}$ events, which one would have expected due to the second tau being independent of the tau from the charged Higgs boson.

Now the amount of possible improvement of the significance can be calculated. Using the gaussian statistics to calculate the change in significance as

| Heavy charged Higgs boson ($m_{H^+}$) | Removed (%) | $\Delta_{sig}$/sig (%) |
|---|---|---|
| 180 | 1.0 | 1.3 |
| 200 | 0.4 | 1.9 |
| 220 | 1.9 | 0.3 |
| 250 | 1.5 | 0.7 |
| 300 | 1.3 | 0.9 |
| 350 | 3.4 | -1.2 |
| 400 | 1.8 | 0.4 |
| 500 | 1.6 | 0.6 |

Table 8.2: The percentages of removed events from the signal and the increase in significance. For the heavy charged Higgs boson, the percentage was calculated in the region $m_{H^+} > 100$ GeV/c$^2$ where the percent of removed $t\bar{t}$ jet background is 4.4%.

$$\begin{aligned} \frac{\Delta_{sig}}{sig} &= \frac{1}{S_1/\sqrt{B_1}} \left( \frac{S_2}{\sqrt{B_2}} - \frac{S_1}{\sqrt{B_1}} \right) \\ &= \frac{1 - r_S}{\sqrt{1 - r_B}} - 1, \end{aligned} \tag{8.2}$$

where $r_S$, $r_B$ are the percentage of events removed from signal and background respectively. The improvements in significance are presented in Tables (8.1) and (8.2) for the light and heavy charged Higgs bosons. The expected limit calculations for the heavy charged Higgs boson cross section before and after the tau veto are presented in Figure 8.6. The tau veto does not have a clear effect on the limits as for some mass points the limits go up while for some the limits go down. The new systematic uncertainties added by the tau veto discussed below were included in the limit calculation.

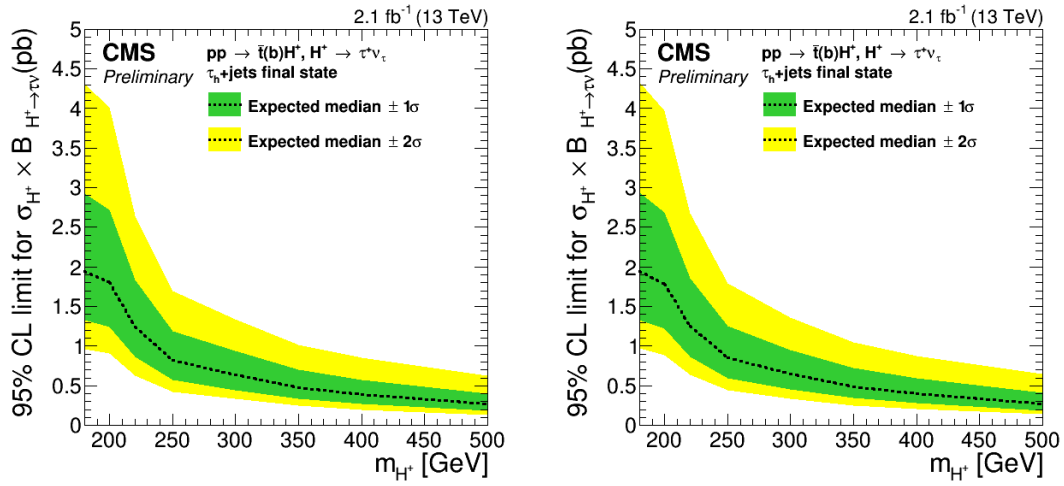


Figure 8.6: The expected $\sigma_{H^+} \times B_{H^+ \to \tau\nu}$ before and after the optimistic veto for the heavy charged Higgs boson. The effect of the veto is barely visible.

| 95% CL upper limit on $\sigma_{H^+} \times B_{H^+ \to \tau\nu}$ | | | | | | |
|---|---|---|---|---|---|---|
| $m_{H^+}$ | Expected limit | | | | | Observed |
| (GeV) | $-2\sigma$ | $-1\sigma$ | median | $+1\sigma$ | $+2\sigma$ | limit |
| 180 | 0.967 | 1.327 | 1.939 | 2.926 | 4.310 | Blinded |
| 200 | 0.903 | 1.238 | 1.808 | 2.718 | 4.012 | Blinded |
| 220 | 0.632 | 0.860 | 1.243 | 1.839 | 2.648 | Blinded |
| 250 | 0.421 | 0.570 | 0.816 | 1.191 | 1.700 | Blinded |
| 300 | 0.331 | 0.447 | 0.641 | 0.935 | 1.338 | Blinded |
| 350 | 0.245 | 0.332 | 0.477 | 0.698 | 1.013 | Blinded |
| 400 | 0.201 | 0.273 | 0.392 | 0.576 | 0.849 | Blinded |
| 500 | 0.135 | 0.184 | 0.268 | 0.403 | 0.625 | Blinded |

Table 8.3: Expected $\sigma_{H^+} \times B_{H^+ \to \tau\nu}$ limits before the optimistic tau veto presented for heavy charged Higgs boson

Adding tau veto introduces new systematic uncertainties to the analysis that need to be taken into account. This tau veto will be affected by the uncertainties in tau identification and the identification of the charged particles whose tracks were used. The systematic uncertainty in $\tau_h$ identification is estimated to be 6% [92]. Uncertainty for the charged pion tracks is taken as 1.4%, as was estimated in [73].

Assuming these uncertainties are fully uncorrelated and summing in quadrature gives the total systematic uncertainty of the tau veto to be 6.2%. Added to the other uncertainties of the analysis presented in Table 8.2, this leads to an increase of 5.6% of the total systematic uncertainty in the analysis.

In the high energy tail, the uncertainties are determined using an exponential fit of the

| 95% CL upper limit on $\sigma_{\mathrm{H}^+} \times B_{H^+ \to \tau\nu}$ | | | | | | |
|---|---|---|---|---|---|---|
| $m_{\mathrm{H}^+}$ | Expected limit | | | | | Observed |
| (GeV) | $-2\sigma$ | $-1\sigma$ | median | $+1\sigma$ | $+2\sigma$ | limit |
| 180 | 0.968 | 1.330 | 1.945 | 2.936 | 4.330 | Blinded |
| 200 | 0.891 | 1.221 | 1.783 | 2.684 | 3.970 | Blinded |
| 220 | 0.636 | 0.867 | 1.254 | 1.857 | 2.681 | Blinded |
| 250 | 0.440 | 0.596 | 0.855 | 1.250 | 1.790 | Blinded |
| 300 | 0.334 | 0.452 | 0.648 | 0.947 | 1.360 | Blinded |
| 350 | 0.252 | 0.342 | 0.492 | 0.722 | 1.053 | Blinded |
| 400 | 0.205 | 0.279 | 0.401 | 0.590 | 0.880 | Blinded |
| 500 | 0.139 | 0.189 | 0.275 | 0.415 | 0.648 | Blinded |

Table 8.4: Expected $\sigma_{H^+} \times B_{H^+ \to \tau\nu}$ limit calculations after the optimistic tau veto presented for heavy charged Higgs boson. The results do not show definitive advantage from using the tau veto as the limits for some mass points grow larger and for some a little smaller.

event yields. The statistical uncertainties in the event yield are of the order of few percent for the signals and around four percent for the $\mathrm{t\bar{t}}$ background [92].

| Uncertainty source | EWK+$\mathrm{t\bar{t}}$ with $\tau_{\mathrm{h}}$ (%) |
|---|---|
| Trigger, approximation in $E_{\mathrm{T}}^{\mathrm{miss}}$ | 12 |
| Trigger, single $\mu$ | 0.1 |
| $\tau_{\mathrm{h}}$ identification | 6.0 |
| $\tau$ energy scale | 5.8 |
| $\mu$ identification | $<$0.1 |
| Multijet contamination | 2.0 |
| W$\to \tau\nu_\tau \to \mu\nu_\mu\nu_\tau$ | 1.2 |
| $\tau$ veto | 6.2 |

Table 8.5: Systematic uncertainties associated with EWK+$\mathrm{t\bar{t}}$ with $\tau_{\mathrm{h}}$ background simulation data. [92]

The analysis of the tau veto performance in the optimistic case presented shows a change in significance between $-1.0\%$ and $0.5\%$ for the light charged Higgs boson and between $-1.2\%$ and $1.9\%$ for the heavy charged Higgs boson, depending on the mass used for the simulation of the dataset. An increase of $5.6\%$ in the total systematic uncertainty of the analysis due to the tau veto is determined. The low increase in significance compared to the potential increase shown by using the generator level information to remove all events with more than one tau is explained by the difficulties in identification of the excessive taus in events. The low transverse momenta is the apparent cause of the problems in the

identification. Even though the signal taus were chosen to be 1-pronged, the other taus in the event can be 3-pronged, so that the spreading of the decay products in the low $p_{\mathrm{T}}$ tau decays hinders their reconstruction.

### 8.1.2 A realistic veto using isolated charged tracks and tau identification

An algorithm for remove multiple tau events in a real analysis could utilize the charged pion tracks in the detector fulfilling isolation conditions. This could notice some of the 1-prong taus that have been missed by the reconstruction algorithm due to too low transverse momenta. Some of the 3-pronged taus with low $p_{\mathrm{T}}$ might not fulfil the isolation conditions due to spreading of the charged decay products.

For the charged pion track, the following conditions are used:

- $p_{\mathrm{T}} \geq 15$ GeV/c.
- Sum of charged track $p_{\mathrm{T}}$ between $0.03 \leq \Delta R \leq 0.1$ around the $\pi^{\pm}$ is than 1 GeV/c.

These conditions lead to a slight improvement in the ratio of events with one tau versus events with multiple taus. This is probably by no means optimal selection of conditions, but as an ideal case was already studied above these conditions mostly serve as an example of how such a tau veto could be constructed. The veto has little to no effect on the fake tau events.

The veto removes of the order of few percent of all the events. The results of this tau veto are shown in the limit calculation for the heavy Higgs scenario in Figures 8.7. No clear improvement in the limits for the cross section is achieved with this tau veto but the uncertainties are increased by introducing the veto into the analysis.

| 95% CL upper limit on $\sigma_{\mathrm{H}^+} \times B_{H^+ \to \tau\nu}$ | | | | | | |
|---|---|---|---|---|---|---|
| $m_{\mathrm{H}^+}$ | Expected limit | | | | | Observed |
| (GeV) | $-2\sigma$ | $-1\sigma$ | median | $+1\sigma$ | $+2\sigma$ | limit |
| 180 | 0.967 | 1.327 | 1.939 | 2.926 | 4.310 | Blinded |
| 200 | 0.903 | 1.238 | 1.808 | 2.718 | 4.012 | Blinded |
| 220 | 0.632 | 0.860 | 1.243 | 1.839 | 2.648 | Blinded |
| 250 | 0.421 | 0.570 | 0.816 | 1.191 | 1.700 | Blinded |
| 300 | 0.331 | 0.447 | 0.641 | 0.935 | 1.338 | Blinded |
| 350 | 0.245 | 0.332 | 0.477 | 0.698 | 1.013 | Blinded |
| 400 | 0.201 | 0.273 | 0.392 | 0.576 | 0.849 | Blinded |
| 500 | 0.135 | 0.184 | 0.268 | 0.403 | 0.625 | Blinded |

Table 8.6: Expected $\sigma_{H^+} \times B_{H^+ \to \tau\nu}$ limit calculation values before the realistic tau veto presented heavy charged Higgs boson

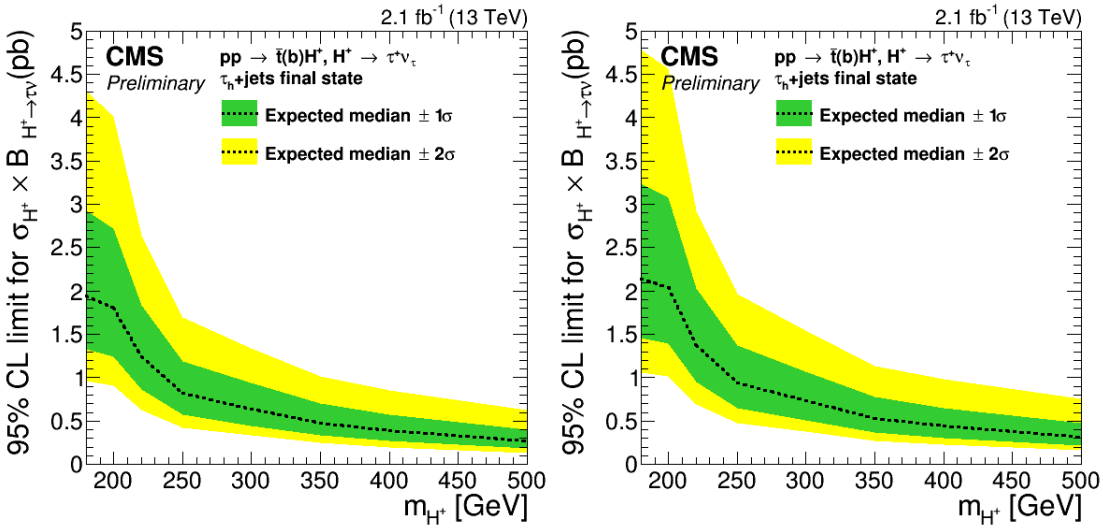


Figure 8.7: The expected $\sigma_{H^+} \times B_{H^+\to\tau\nu}$ before and after the realistic veto for the heavy charged Higgs boson. The limits become worse with the added veto.

| 95% CL upper limit on $\sigma_{H^+} \times B_{H^+\to\tau\nu}$ | | | | | | |
|---|---|---|---|---|---|---|
| $M_{H^+}$ | Expected limit | | | | | Observed |
| (GeV) | $-2\sigma$ | $-1\sigma$ | median | $+1\sigma$ | $+2\sigma$ | limit |
| 180 | 1.064 | 1.462 | 2.139 | 3.237 | 4.785 | Blinded |
| 200 | 1.018 | 1.395 | 2.042 | 3.082 | 4.564 | Blinded |
| 220 | 0.696 | 0.948 | 1.370 | 2.031 | 2.929 | Blinded |
| 250 | 0.482 | 0.653 | 0.937 | 1.371 | 1.961 | Blinded |
| 300 | 0.377 | 0.511 | 0.732 | 1.072 | 1.542 | Blinded |
| 350 | 0.271 | 0.368 | 0.529 | 0.776 | 1.130 | Blinded |
| 400 | 0.227 | 0.308 | 0.444 | 0.654 | 0.980 | Blinded |
| 500 | 0.160 | 0.219 | 0.318 | 0.481 | 0.754 | Blinded |

Table 8.7: Expected $\sigma_{H^+} \times B_{H^+\to\tau\nu}$ limit calculation values after the realistic tau veto presented heavy charged Higgs boson. The tau veto does not improve the limits on the cross section.

# Chapter 9

# Conclusions

Excessive neutrinos in the events deteriorate the mass measurement of the charged Higgs boson signal in the $\tau\nu$ -channel. Neutrinos from other decays than the charged Higgs boson signal affect the amount and direction of the missing transverse energy $E_{\mathrm{T}}^{\mathrm{miss}}$ in the collision, distorting the transverse mass reconstructions that use the signal tau and missing energy. Any events containing more than one tau will reduce the accuracy of the reconstruction.

The effectiveness in reducing EWK+$\mathrm{t\bar{t}}$ jets with genuine tau background in the charged Higgs boson signal regions by removing events with multiple taus was shown using generator level information in simulated collision data. The achieved reduction in this background was 43% and 26% in the regions $m_{\mathrm{T}} \geq 100$ GeV/c$^2$ and $m_{\mathrm{T}} = 60 - 180$ GeV/c$^2$ respectively when using reconstructed taus for calculating the transverse masses.

This potential is hard to realize in the analysis of real data due to the inefficiency of tau reconstruction algorithms when searching for multiple tau events, as the sub-leading tau can be very soft. From the generator level information the sources for the difficulties in identifying the excessive taus were shown to be the low $p_{\mathrm{T}}$ and the related large spread in the decay products of the taus.

An optimal case scenario was presented and analysed, assuming all charged tracks within $\Delta R \leq 0.1$ of the direction of unidentified taus could be used to identify the tau. A reduction of $\mathrm{t\bar{t}}$ background of 2.2% and 4.4% in the signal regions for light and heavy charged Higgs boson was shown. Combined with the reductions in the signal events the change in significance was $\Delta_{\mathrm{sig}} \in [-1.0\%, 0.5\%]$ for the light charged Higgs boson and as $\Delta_{\mathrm{sig}} \in [-1.2\%, 1.9\%]$ for the heavy charged Higgs boson. A realistic implementation of a tau veto was also presented. The increase in the systematic uncertainty of the analysis was determined by the systematic uncertainties in tau identification and the track reconstructions. The uncertainty contributed by the tau veto to the analysis was estimated to be 6.2%. This leads to an increase of 5.6% for the overall analysis.

These considerations lead to the conclusion that even though removing the events with more than one tau has great potential in improving the analysis, the difficulties in reconstructing and identifying these excess taus from the collision data renders this approach moot. As the increase of systematic uncertainty in implementing the tau veto is larger than the improvement in significance, it would not benefit the analysis. More accurate methods for reconstructing the low $p_{\mathrm{T}}$ taus in the CMS data are required in order to make vetoing the events with more than one tau useful in this analysis.

# Bibliography


[1] CMS Collaboration. Observation of a new boson at a mass of 125 gev with the cms experiment at the lhc. *Phys. Lett. B*, 716(30), 2012.

[2] ATLAS Collaboration. Observation of a new particle in the search for the Standard Model Higgs boson with the ATLAS detector at the LHC. *Phys. Lett. B*, 716(30), 2012.

[3] E. Noether. Invariante Variationsprobleme. *Nachr. d. König. Gesellsch. d. Wiss. zu Göttingen*, 1918.

[4] M. Peskin & D. Schroeder. *An introduction to quantum field theory.* Perseus Books Publishing, 1995.

[5] G. T'Hooft. Renormalization of massless Yang-Mills fields. *Nucl. Phys. B*, 33(1):173–199, 1971.

[6] M. Kobayashi & T. Maskawa. CP-Violation in the Renormalizable Theory of Weak Interaction. *Progr. Theor. Exp. Phys.*, 49(2):652, 1973.

[7] M. Perl et al. Evidence for Anomalous Lepton Production in $e^-e^+$ Annihilation. *Phys. Rev. Lett.*, 35(22), 1975.

[8] M. Perl. Review of Heavy Lepton Production in $e^-e^+$ Annihilation. *SLAC-PUB-2022*, 1977.

[9] S. Herb et al., J. Appel et al., A. Ito et al. Observation of a Dimuon Resonance at 9.5 GeV in 400-GeV Proton-Nucleus Collisions. *Phys. Rev. Lett.*, 35(22), 1975.

[10] F. Abe et al. (CDF Collaboration). Observation of Top Quark Production in pp Collisions with the Collider Detector at Fermilab. *Phys. Rev. Lett.*, 74(14):2626–2631, 1995.

[11] MissMJ. Standard Model of Elementary Particles, PBS NOVA, Fermilab, 23.1.2016.

[12] P. Dirac. The Quantum Theory of the Emission and Absorption of Radiation. *Proc. of the Roy. Soc. A*, 114(767):243–265, 1927.

[13] S. Tomonaga. On a Relativistically Invariant Formulation of the Quantum Theory of Wave Fields. *Prog. Theor. Phys.*, 1(2):27–43, 1946.

[14] R. Feynman. Relativistic Cut-Off for classical electrodynamics. *Phys. Rev.*, 74(8):939–947, 1948.

[15] J. Schwinger. Quantum Electrodynamics I. A covariant formulation. *Phys. Rev.*, 74(8):1439–1462, 1948.

[16] T. Tati & S. Tomonaga. A Self-Consistent Subtraction Method in the Quantum Field Theory. *Prog. Theor. Phys*, 3(4):391–407, 1948.

[17] T. Tati & S. Tomonaga. The Quantum Theory of Electron. *Proc. of the Roy. Soc. A*, 117:610–625, 1928.

[18] F.Wilson. Fermi's Theory of Beta Decay (translation of the original paper in 1933). *Am. J. Phys.*, 36(12):1150, 1968.

[19] T. D. Lee and C. N. Yang. Question of parity conservation in weak interactions. *Phys. Rev.*, 104:254–258, Oct 1956.

[20] J. H. Christenson, J. W. Cronin, V. L. Fitch, and R. Turlay. Evidence for the $2\pi$ decay of the $k_2^0$ meson. *Phys. Rev. Lett.*, 13:138–140, Jul 1964.

[21] G. Passaleva and G. J. Bobbink. Tests of lepton universality in $\tau$ decays. In *High-energy physics. Proceedings, 29th International Conference, ICHEP'98, Vancouver, Canada, July 23-29, 1998. Vol. 1, 2*, 1998.

[22] J. Bardeen, L. N. Cooper, and J. R. Schrieffer. Microscopic theory of superconductivity. *Phys. Rev.*, 106:162–164, Apr 1957.

[23] Y. Nambu and G. Jona-Lasinio. Dynamical model of elementary particles based on an analogy with superconductivity. i. *Phys. Rev.*, 122:345–358, Apr 1961.

[24] Y. Nambu and G. Jona-Lasinio. Dynamical model of elementary particles based on an analogy with superconductivity. ii. *Phys. Rev.*, 124:246–254, Oct 1961.

[25] G. S. Guralnik, C. R. Hagen, and T. W. B. Kibble. Global conservation laws and massless particles. *Phys. Rev. Lett.*, 13:585–587, Nov 1964.

[26] F. Englert and R. Brout. Broken symmetry and the mass of gauge vector mesons. *Phys. Rev. Lett.*, 13:321–323, Aug 1964.

[27] Peter W. Higgs. Broken symmetries and the masses of gauge bosons. *Phys. Rev. Lett.*, 13:508–509, Oct 1964.

[28] Nobel Media Ab. The Nobel Prize in Physics 2013, 26. Jan. 2016.

[29] J. Goldstone. Field Theories with Superconductor Solutions. *Nuovo Cim.*, 19:154–164, 1961.

[30] S. F. Novaes. Standard model: An Introduction. In *Particles and fields. Proceedings, 10th Jorge Andre Swieca Summer School, Sao Paulo, Brazil, February 6-12, 1999*, 1999.

[31] S. L. Glashow. Partial Symmetries of Weak Interactions. *Nucl. Phys.*, 22:579–588, 1961.

[32] Steven Weinberg. A model of leptons. *Phys. Rev. Lett.*, 19:1264–1266, Nov 1967.

[33] Abdus Salam. Weak and Electromagnetic Interactions. *Conf. Proc.*, C680519:367–377, 1968.

[34] W. Cottingham & D. Greenwood. *An introduction to the Standard Model of particle physics, 2nd ed.* Cambridge University Press, 2007.

[35] H. David Politzer. Reliable perturbative results for strong interactions? *Phys. Rev. Lett.*, 30:1346–1349, Jun 1973.

[36] David J. Gross and Frank Wilczek. Ultraviolet behavior of non-abelian gauge theories. *Phys. Rev. Lett.*, 30:1343–1346, Jun 1973.

[37] Jan Smit. *Introduction to quantum fields on a lattice, 1 ed.* Cambridge University Press, 2012.

[38] Y. Fukuda, T. Hayakawa, E. Ichihara, K. Inoue, K. Ishihara, H. Ishino, Y. Itow, T. Kajita, J. Kameda, S. Kasuga, K. Kobayashi, Y. Kobayashi, Y. Koshio, M. Miura, M. Nakahata, S. Nakayama, A. Okada, K. Okumura, N. Sakurai, M. Shiozawa, Y. Suzuki, Y. Takeuchi, Y. Totsuka, S. Yamada, M. Earl, A. Habig, E. Kearns, M. D. Messier, K. Scholberg, J. L. Stone, L. R. Sulak, C. W. Walter, M. Goldhaber, T. Barszczxak, D. Casper, W. Gajewski, P. G. Halverson, J. Hsu, W. R. Kropp, L. R. Price, F. Reines, M. Smy, H. W. Sobel, M. R. Vagins, K. S. Ganezer, W. E. Keig, R. W. Ellsworth, S. Tasaka, J. W. Flanagan, A. Kibayashi, J. G. Learned, S. Matsuno, V. J. Stenger, D. Takemori, T. Ishii, J. Kanzaki, T. Kobayashi, S. Mine, K. Nakamura, K. Nishikawa, Y. Oyama, A. Sakai, M. Sakuda, O. Sasaki, S. Echigo, M. Kohama, A. T. Suzuki, T. J. Haines, E. Blaufuss, B. K. Kim, R. Sanford, R. Svoboda, M. L. Chen, Z. Conner, J. A. Goodman, G. W. Sullivan, J. Hill, C. K. Jung, K. Martens, C. Mauger, C. McGrew, E. Sharkey, B. Viren, C. Yanagisawa, W. Doki, K. Miyano, H. Okazawa, C. Saji, M. Takahata, Y. Nagashima, M. Takita, T. Yamaguchi, M. Yoshida, S. B. Kim, M. Etoh, K. Fujita, A. Hasegawa, T. Hasegawa, S. Hatakeyama, T. Iwamoto, M. Koga, T. Maruyama, H. Ogawa, J. Shirai, A. Suzuki, F. Tsushima, M. Koshiba, M. Nemoto, K. Nishijima, T. Futagami, Y. Hayato, Y. Kanaya, K. Kaneyuki, Y. Watanabe, D. Kielczewska, R. A. Doyle, J. S. George, A. L. Stachyra, L. L. Wai, R. J. Wilkes, and K. K. Young. Evidence for oscillation of atmospheric neutrinos. *Phys. Rev. Lett.*, 81:1562–1567, Aug 1998.

[39] Nobel Media AB. The Nobel Prize in Physics 2015, 7. Jan. 2016.

[40] U. Sarkar. *Particle and Astroparticle Physics, 1 ed.* CRC Press, 2007.

[41] U. Sarkar. *Particle and Astroparticle Physics, 1 ed.* CRC Press, 2007.

[42] Sidney Coleman and Jeffrey Mandula. All possible symmetries of the $s$ matrix. *Phys. Rev.*, 159:1251–1256, Jul 1967.

[43] Stephen P. Martin. A Supersymmetry primer. pages 30–51, 1997. [Adv. Ser. Direct. High Energy Phys.18,1(1998)].

[44] Jean-Loup Gervais and B. Sakita. Field Theory Interpretation of Supergauges in Dual Models. *Nucl. Phys.*, B34:632–639, 1971.

[45] Yu. A. Golfand and E. P. Likhtman. Extension of the Algebra of Poincare Group Generators and Violation of p Invariance. *JETP Lett.*, 13:323–326, 1971. [Pisma Zh. Eksp. Teor. Fiz.13,452(1971)].

[46] D. V. Volkov and V. P. Akulov. Possible universal neutrino interaction. *JETP Lett.*, 16:438–440, 1972. [Pisma Zh. Eksp. Teor. Fiz.16,621(1972)].

[47] Pierre Fayet. Spontaneously Broken Supersymmetric Theories of Weak, Electromagnetic and Strong Interactions. *Phys. Lett.*, B69:489, 1977.

[48] Ian J. R. Aitchison. Supersymmetry and the MSSM: An Elementary introduction. 2005.

[49] M. Cahill-Rowley, J. L. Hewett, A. Ismail, and T. G. Rizzo. Lessons and prospects from the pMSSM after LHC Run I. *Phys. Rev.*, D91(5):055002, 2015.

[50] John F. Gunion, Howard E. Haber, Gordon L. Kane, and Sally Dawson. The Higgs Hunter's Guide. *Front. Phys.*, 80:1–448, 2000.

[51] Abdelhak Djouadi. The Anatomy of electro-weak symmetry breaking. II. The Higgs bosons in the minimal supersymmetric model. *Phys. Rept.*, 459:1–241, 2008.

[52] Matthias Schott and Monica Dunford. Review of single vector boson production in pp collisions at $\sqrt{s} = 7$ TeV. *Eur. Phys. J.*, C74:2916, 2014.

[53] Vardan Khachatryan et al. Measurements of Inclusive $W$ and $Z$ Cross Sections in $pp$ Collisions at $\sqrt{s} = 7$ TeV. *JHEP*, 01:080, 2011.

[54] E. D. Bloom, D. H. Coward, H. DeStaebler, J. Drees, G. Miller, L. W. Mo, R. E. Taylor, M. Breidenbach, J. I. Friedman, G. C. Hartmann, and H. W. Kendall. High-energy inelastic $e - p$ scattering at 6° and 10°. *Phys. Rev. Lett.*, 23:930–934, Oct 1969.

[55] John C. Collins, Davison E. Soper, and George F. Sterman. Factorization of Hard Processes in QCD. *Adv. Ser. Direct. High Energy Phys.*, 5:1–91, 1989.

[56] R. P. Feynman. THE BEHAVIOR OF HADRON COLLISIONS AT EXTREME ENERGIES. 1989.

[57] Yuri L. Dokshitzer. Calculation of the Structure Functions for Deep Inelastic Scattering and e+ e- Annihilation by Perturbation Theory in Quantum Chromodynamics. *Sov. Phys. JETP*, 46:641–653, 1977. [Zh. Eksp. Teor. Fiz.73,1216(1977)].

[58] V. N. Gribov and L. N. Lipatov. Deep inelastic e p scattering in perturbation theory. *Sov. J. Nucl. Phys.*, 15:438–450, 1972. [Yad. Fiz.15,781(1972)].

[59] Guido Altarelli and G. Parisi. Asymptotic Freedom in Parton Language. *Nucl. Phys.*, B126:298, 1977.

[60] *ECFA-CERN Workshop on large hadron collider in the LEP tunnel, Lausanne and CERN, Geneva, Switzerland, 21-27 Mar 1984: Proceedings. 1.*, 1984.

[61] Thomas Sven Pettersson and P Lefèvre. The Large Hadron Collider: conceptual design. Technical Report CERN-AC-95-05-LHC, CERN, Geneva, Oct 1995.

[62] Science & Technology Facility Council, 22.02.2016.

[63] M. Della Negra et al. CMS: The Compact Muon Solenoid: Letter of intent for a general purpose detector at the LHC. 1992.

[64] S. Chatrchyan et al. The CMS experiment at the CERN LHC. *JINST*, 3:S08004, 2008.

[65] Marzena Lapka. Interactive Slice of the CMS detector, 10.7.2015.

[66] Serguei Chatrchyan et al. Description and performance of track and primary-vertex reconstruction with the CMS tracker. *JINST*, 9(10):P10009, 2014.

[67] V. Veszpremi. Operation and performance of the CMS tracker. *JINST*, 9:C03005, 2014.

[68] Serguei Chatrchyan et al. Energy Calibration and Resolution of the CMS Electromagnetic Calorimeter in *pp* Collisions at $\sqrt{s} = 7$ TeV. *JINST*, 8:P09009, 2013. [JINST8,9009(2013)].

[69] CMS Collaboration. *CMS Physics: Technical Design Report Volume 1: Detector Performance and Software*. Technical Design Report CMS. CERN, Geneva, 2006.

[70] Serguei Chatrchyan et al. Performance of CMS muon reconstruction in *pp* collision events at $\sqrt{s} = 7$ TeV. *JINST*, 7:P10002, 2012.

[71] Giovanni Petrucciani, Andrea Rizzi, and Carl Onni Urho Vuosalo. Mini-AOD: A New Analysis Data Format for CMS. A new analysis data format for CMS. Technical Report CMS-CR-2015-052. 7, CERN, Geneva, May 2015.

[72] Particle-Flow Event Reconstruction in CMS and Performance for Jets, Taus, and MET. Technical Report CMS-PAS-PFT-09-001, CERN, 2009. Geneva, Apr 2009.

[73] Measurement of Tracking Efficiency. Technical Report CMS-PAS-TRK-10-002, CERN, 2010. Geneva, 2010.

[74] Performance of muon identification in pp collisions at s**0.5 = 7 TeV. 2010.

[75] Wolfgang Adam, R Frühwirth, Are Strandlie, and T Todor. Reconstruction of Electrons with the Gaussian-Sum Filter in the CMS Tracker at the LHC. Technical Report CMS-NOTE-2005-001, CERN, Geneva, Jan 2005.

[76] Studies of Tracker Material. Technical Report CMS-PAS-TRK-10-003, 2010.

[77] Isolated Photon Reconstruction and Identification at sqrts. Technical Report CMS-PAS-EGM-10-006, CERN, Geneva, 2011.

[78] K. Rose. Deterministic annealing for clustering, compression, classification, regression, and related optimization problems. *Proceedings of the IEEE*, 86(11):2210–2239, Nov 1998.

[79] Matteo Cacciari, Gavin P. Salam, and Gregory Soyez. The Anti-k(t) jet clustering algorithm. *JHEP*, 04:063, 2008.

[80] Jet Performance in pp Collisions at 7 TeV. Technical Report CMS-PAS-JME-10-003, CERN, Geneva, 2010.

[81] CMS Collaboration. Determination of jet energy calibration and transverse momentum resolution in CMS. *Journal of Instrumentation*, 6:11002, November 2011.

[82] Performance of b tagging at sqrt(s)=8 TeV in multijet, ttbar and boosted topology events. Technical Report CMS-PAS-BTV-13-001, CERN, Geneva, 2013.

[83] CMS Collaboration. Missing transverse energy performance of the CMS detector. *Journal of Instrumentation*, 6:9001, September 2011.

[84] K. A. Olive et al. Review of Particle Physics. *Chin. Phys.*, C38:090001, 2014.

[85] Vardan Khachatryan et al. Reconstruction and identification of $\tau$ lepton decays to hadrons and $\nu_\tau$ at CMS. *JINST*, 11(01):P01019, 2016.

[86] L. Lusito. Reconstruction and identification of hadronic Tau decays with the CMS detector, talk at Ch$^{\pm}$arged '08, 16.-19.9.2008.

[87] Andre G. Holzner. Searches for charged Higgs bosons at LEP. In *36th Rencontres de Moriond on Electroweak Interactions and Unified Theories Les Arcs, France, March 10-17, 2001*, 2001.

[88] ALEPH Collaboration. Search for charged Higgs bosons in $e^+e^-$ collisions at energies up to $\sqrt{s} = 209$ GeV. *Phys. Lett. B*, 543(1), 2002.

[89] J. Abdallah et al. Search for charged Higgs bosons at LEP in general two Higgs doublet models. *Eur. Phys. J.*, C34:399–418, 2004.

[90] OPAL Collaboration. Search for charged Higgs boson in $e^+e^-$ collisions at energies up to $\sqrt{s} = 189$GeV - 209 GeV. *Eur. Phys. J. C*, 72(2076), 2012.

[91] Robert Harlander, Michael Kramer, and Markus Schumacher. Bottom-quark associated Higgs-boson production: reconciling the four- and five-flavour scheme approach. 2011.

[92] Search for charged Higgs bosons with the H+ to tau nu decay channel in the fully hadronic final state at sqrt s = 8 TeV. Technical Report CMS-PAS-HIG-14-020, CERN, Geneva, 2014.

[93] Erik Pekkarinen. Data-driven measurement of the background with misidentified tau leptons in a search for charged Higgs boson. *Master's Thesis, Aalto University*, 2015.

[94] Paolo Azzurri. Track Reconstruction Performance in CMS. *Nucl. Phys. Proc. Suppl.*, 197:275–278, 2009.

[95] Vardan Khachatryan et al. Performance of Electron Reconstruction and Selection with the CMS Detector in Proton-Proton Collisions at $\sqrt{s} = 8$ TeV. *JINST*, 10(06):P06005, 2015.

# Appendix

## A. Plots for $H^+$ transverse masses using reconstructed taus

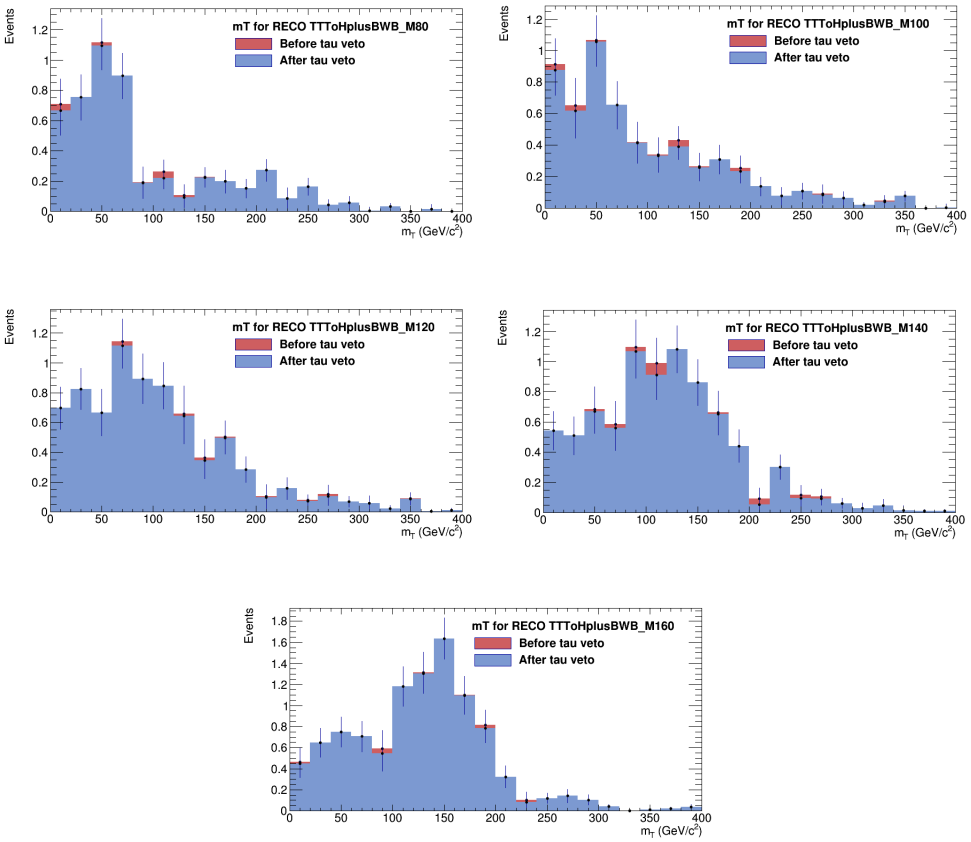


Figure A1: Transverse masses for the light charged Higgs boson signals using reconstructed taus in the mass region 80-160 GeV/$c^2$, presented before and after the tau veto using the charged tracks.

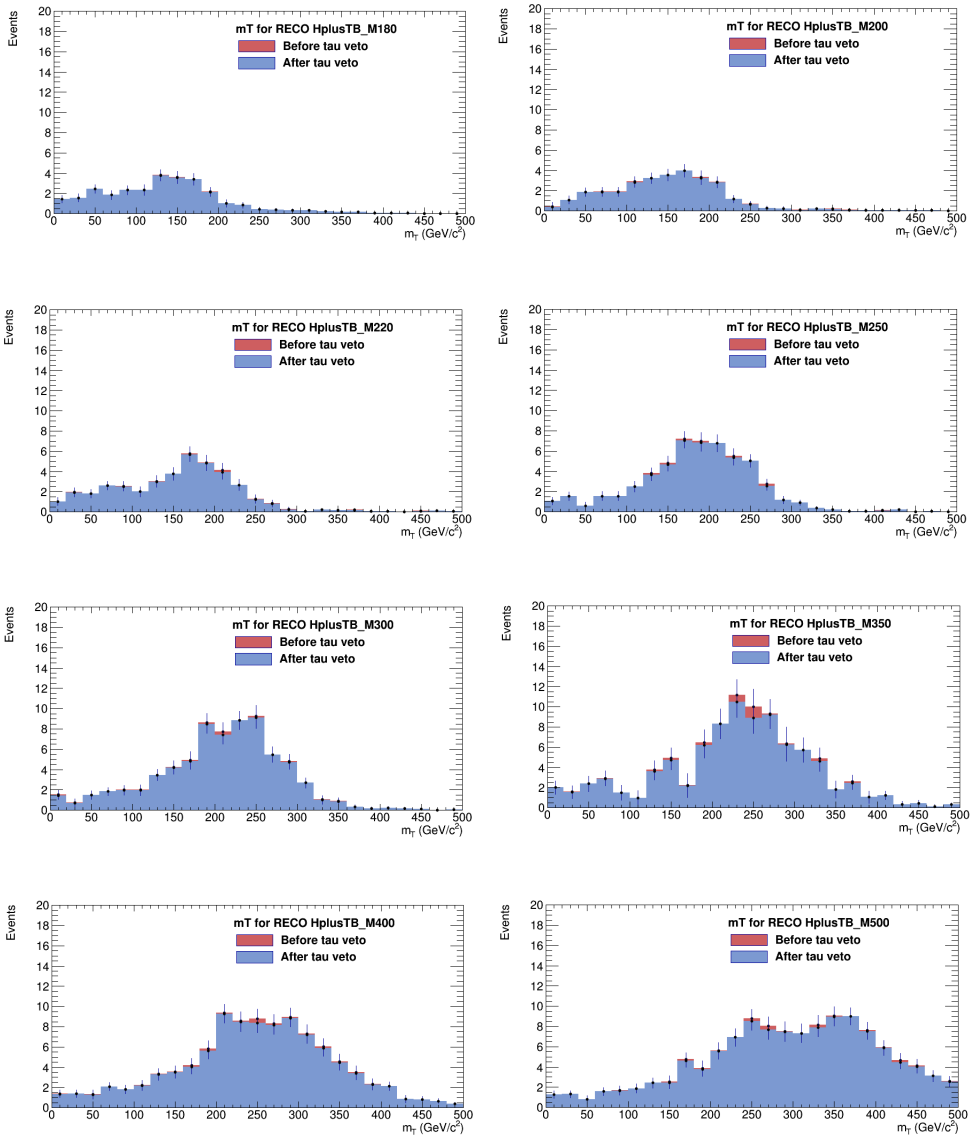


Figure A2: Transverse masses for the heavy charged Higgs boson signals using reconstructed taus in the mass region 180-500 GeV/$c^2$, presented before and after the tau veto using the charged tracks.